Generalized Monte Carlo Tool for Investigating Low-Field and High Field Properties of Materials Using Non-parabolic Band Structure Model

by

Raghuraj Hathwar

A Thesis Presented in Partial Fulfillment
of the Requirements for the Degree
Master of Science

Approved June 2011 by the
Graduate Supervisory Committee:

Dragica Vasileska, Chair
Stephen Marshall Goodnick
Marco Saraniti

ARIZONA STATE UNIVERSITY

August 2011

ABSTRACT

In semiconductor physics, many properties or phenomena of materials can be brought to light through certain changes in the materials. Having a tool to define new material properties so as to highlight certain phenomena greatly increases the ability to understand that phenomena. The generalized Monte Carlo tool allows the user to do that by keeping every parameter used to define a material, within the non-parabolic band approximation, a variable in the control of the user. A material is defined by defining its valleys, energies, valley effective masses and their directions. The types of scattering to be included can also be chosen. The non-parabolic band structure model is used.

With the deployment of the generalized Monte Carlo tool onto www.nanoHUB.org the tool will be available to users around the world. This makes it a very useful educational tool that can be incorporated into curriculums. The tool is integrated with Rappture, to allow user-friendly access of the tool. The user can freely define a material in an easy systematic way without having to worry about the coding involved. The output results are automatically graphed and since the code incorporates an analytic band structure model, it is relatively fast.

The versatility of the tool has been investigated and has produced results closely matching the experimental values for some common materials. The tool has been uploaded onto www.nanoHUB.org by integrating it with the Rappture

interface. By using Rappture as the user interface, one can easily make changes to the current parameter sets to obtain even more accurate results.

ACKNOWLEDGMENTS

I am deeply indebted to my guide and mentor, Dr. Dragica Vasileska. Without her support, advice and optimism this work would not have been possible. Her expertise in the area helped me to quickly acquire the knowledge I needed to complete this thesis. I am also grateful for the time and energy she devoted in discussing my research and editing my thesis.

I am grateful to Dr. Stephen Goodnick and Dr. Marco Saraniti for being a part of my Graduate Advisory Committe. I would like to extend my appreciation to the School of Electrical, Computer and Energy Engineering at Arizona State University for providing me this opportunity to pursue my Master's degree. I also take this opportunity to thank Darleen Mandt and Esther Korner for helping me with all the official documents.

I would like to thank all my colleagues in the Computational Electronics group for their help. I am totally indebted to my family for the love and support I received in my quest for higher education.

TABLE OF CONTENTS

Page

PAGE

LIST OF FIGURES

Figure Page

CHAPTER 1. INTRODUCTION

1.1. Introduction

Semiconductors have been the focal point of study for electrical transport from the 20th century onwards. The main attraction towards these materials was the ability to change the conductivity of the semiconductor by introducing dopants and also by applying an electric field. Although the main use of semiconductor materials in devices started with the invention of the transistor, it was not the first device to use semiconductors. Metal rectifiers and detectors in radios called 'Cat Whiskers', which were primitive forms of modern day Schottky diodes, were quite common in the beginning of the 20th century [1]. The investigation of semiconductor materials could be said to have started with Russell Ohl of Bell Laboratories when he tried to grow pure crystals of these semiconductors and analyze their properties. These tests led to the realization of a diode structure to alter the electrical properties of a material. Building on the knowledge of how those diodes work, William Schockley, John Bardeen and Walter Brattain sandwiched two diodes together to create the first transistor in 1947 at Bell Labs. Since then the number of different semiconductor materials has grown immensely to produce a variety of devices exploiting the individual, unique advantages of these materials. The experimental success of the semiconductor industry would not have been successful without the corresponding success in the understanding of the physical properties such as the electrical and optical properties of these devices. These properties were

investigated in detail in the 1950's itself [2], leading to the understanding of the energy band structures. From a greater understanding of band structures and other transport properties of these materials, the electrical properties of the devices created closely followed the theories proposed at that time.

1.2. Need for High Field Study

The study of charge transport in semiconductors is of fundamental importance both from the point of view of the basic physics and for its applications to electrical devices [3]. As the need for electrical appliances grew the need for smaller and faster devices grew as well. As can be seen in Figure 1.1 the number of transistors in a device grew at an amazing rate closely following Moore's law [4].

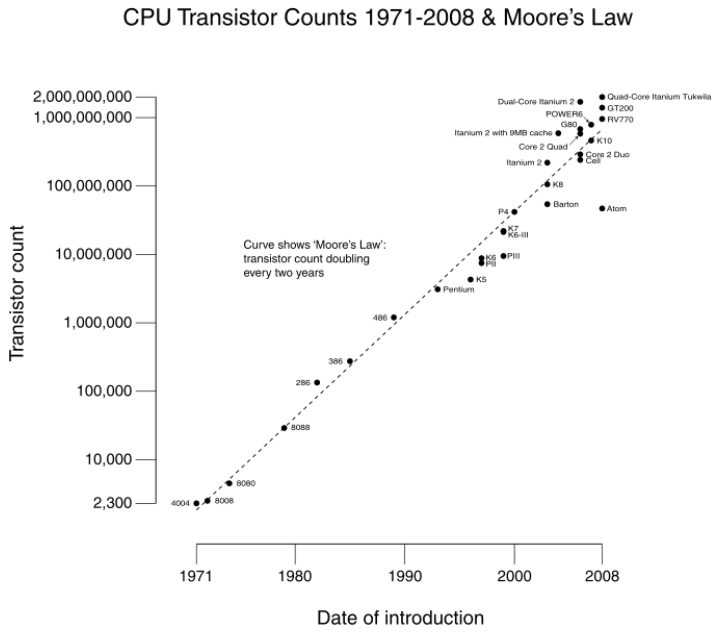

Figure 1.1 CPU Transistor counts (from www.intel.com)

This was made possible by the reduction in the size of the devices. Since the voltage applied across the devices did not reduce at the same rate, the field applied across the device increased. Soon after the invention of the transistor in 1947 it was recognized that electric field strengths, so high so as to cause the devices to no longer obey Ohm's Law, were encountered in semiconductor samples [5-6]. As the requirement of having such high electric fields in commercial transistors became a possibility the need for new physics to tackle the working of these devices arose. The field of nonlinear transport which had been initiated by Landau and Kompanejez [7] entered a period of rapid development soon after the invention of the transistor and a number of researchers devoted their efforts to improving the scientific knowledge of this subject. The surge in research in this field gave way to the realization of new phenomena like the Gunn Effect [8] which then led to the invention of new devices like the transit-time device.

1.3. Advantages of the Monte Carlo method

Analyzing charge transport at high electric fields in devices operated in the on-state is a difficult problem both from the mathematical and physical point of view. The Boltzmann equation which defines the transport phenomena for semi-classical cases is a complicated integro-differential equation. Analytic solutions of the Boltzmann equation can only be obtained for very few cases and are usually not applicable to real systems. In order to get an analytic result it is

necessary to use such drastic approximations that it can no longer be considered appropriate to describe real device operation. In 1966 Kurosawa proposed the Monte Carlo technique [9] and Budd proposed the iterative technique [10]. With these techniques it became clear that, with the use of modern computers, it would be possible to exactly solve the Boltzmann equation numerically for physical models of considerable complexity. These two techniques were then developed further by Price [11], Rees [12] and Fawcett [13]. The Monte Carlo method became the more popular technique because it is easier to use and has more physically interpretable results.

Low field properties of the semiconductor can be investigated using the relaxation time approximation (RTA) for the case when the relevant scattering processes are either elastic or isotropic. If that is not the case, then Rode's iterative procedure has to be used [14]. The Monte Carlo method which can be used for calculation of low-field and high-field properties of a semiconductor uses a different methodology. In fact, in the long-time limit the Monte Carlo method gives the solution of the Boltzmann Transport Equation (BTE). In the short-time limit, the Monte Carlo method gives the solution of the Prigogine equation. Monte Carlo techniques are statistical numerical methods, which are applied to the simulation of random processes. In fact the Monte Carlo method as a statistical numerical method was born well before its application to transport problems [15] and has been applied to a number of scientific fields [16-17]. In case of the charge transport however the solution of the Boltzmann transport equation is a direct

simulation of the dynamics of the carriers in the material. This means that while the simulation is being run, while the solution is being built up, any physical information can be easily extracted. Therefore, even though the result of the Monte Carlo simulation requires a correct physical interpretation, the method is a very useful tool to achieve real solutions. It permits the simulation of particular physical situations unattainable in experiments, or even investigation of nonexistent materials in order to emphasize special features of the phenomenon under study. This use of the Monte Carlo technique makes it similar to an experimental technique and can be compared with analytically formulated theory.

A brief overview of the different types of Monte Carlo methods used in device simulation and their implementation is discussed in Chapter 2. Also in Chapter 2, the common types of scattering processes and their corresponding scattering rates derived using the non-parabolic band structure are discussed. In Chapter 3, the generalized Monte Carlo method for any material and its implementation is discussed. Simulation results for some common materials like Silicon, Germanium and Gallium Arsenide obtained using the generalized Monte Carlo code and are compared with experimental data in Chapter 4. In Chapter 5, the rapture interface which enables the implementation of the code onto www.nanoHUB.org is discussed along with some details of its user interface. Conclusions derived from this research and future directions of research are given in Chapter 6.

CHAPTER 2. THE MONTE CARLO METHOD

2.1. Introduction

The purpose of device modeling is to be able to predict the electrical properties of materials and devices. This would then permit changing certain parameters to improve performance. To obtain these electrical properties, one needs to know the behavior of the particles in the devices, or more specifically in the materials used in those devices. The Boltzmann transport equation [18-19] ,

$$\frac{\partial f}{\partial t} + \boldsymbol{v}.\nabla_r f + \boldsymbol{F}.\nabla_p f = s(\boldsymbol{r},\boldsymbol{p},t) + \frac{df}{dt}|_{coll} \tag{2.1}$$

is used to obtain this behavior. It governs the carrier transport in materials under the semi-classical approximation. This equation is essentially a conservation of volumes in phase space. The left hand side of equation (2.1) consists of three terms, the first term describes the temporal variation of the distribution function, the second term describes the spatial variation of the distribution function which may arise due to temperature or concentration gradients, and finally the third term describes the effect on the distribution function due to applied fields (electric or magnetic). On the right hand side we have two terms, the first term describes the recombination and generation processes and the second term is the collision integral which describes the scattering processes. As can be seen the Boltzmann transport equation is a complicated integro-differential equation which if needs to be solved analytically, it requires many simplifying assumptions which may not hold in real devices as was mentioned earlier.

The Monte Carlo method is a stochastic method used to solve the Boltzmann transport equation. In order to develop this approach we first write the Boltzmann equation as in [18],

$$\left(\frac{\partial}{\partial t} + e\boldsymbol{E}.\frac{\partial}{\partial \boldsymbol{p}} + \boldsymbol{v}.\boldsymbol{\nabla}\right) f(\boldsymbol{p},\boldsymbol{r},t) \tag{2.2}$$

$$= -\Gamma_{\mathrm{O}} f(\boldsymbol{p},\boldsymbol{r},t) + \int d\boldsymbol{p}' W(\boldsymbol{p},\boldsymbol{p}') f(\boldsymbol{p}',\boldsymbol{r},t)$$

where

$$\Gamma_{\mathrm{O}} = \int d\boldsymbol{p}' W(\boldsymbol{p}',\boldsymbol{p}) \tag{2.3}$$

is the total scattering rate out of state **p** for all scattering processes. This motion of the distribution function is described in six plus one-dimensional phase space, three in momentum, three in real space and one in time. It is therefore convenient to describe the motion of the distribution function along a trajectory in phase space. The variable along this trajectory is taken to be *s* and each coordinate can be parameterized as a function of this variable as

$$\boldsymbol{r} \to \boldsymbol{x}^*(s), \quad \boldsymbol{p} = \hbar\boldsymbol{k} \to \boldsymbol{p}^*(s), \quad t \to s \tag{2.4}$$

and the partial derivatives are constrained by the relationships

$$\frac{d\boldsymbol{x}^*}{ds} = \boldsymbol{v} \;\; and \;\; \frac{d\boldsymbol{p}^*}{ds} = e\boldsymbol{E} \tag{2.5}$$

Applying these changes to equation (2.2) we get

$$\frac{df}{ds} + \Gamma_{\mathrm{O}} f = \int d\boldsymbol{p}' W(\boldsymbol{p},\boldsymbol{p}') f(\boldsymbol{p}') \tag{2.6}$$

Equation (2.6) is a standard differential equation which can be solved using an integrating factor which gives

$$f(\boldsymbol{p},t) = f(\boldsymbol{p},0)\exp\left(\int_0^t \Gamma_O ds'\right) + \int_0^t ds \int d\boldsymbol{p}' W(\boldsymbol{p},\boldsymbol{p}')\, f(\boldsymbol{p}',s)\exp\left(-\int_0^t \Gamma_O ds'\right) \tag{2.7}$$

By a change of variables from $\boldsymbol{p}'(s) \rightarrow \boldsymbol{p}'(t) - e\boldsymbol{E}s$, the above equation becomes

$$f(\boldsymbol{p},t) = f(\boldsymbol{p},0)\exp\left(\int_0^t \Gamma_O ds'\right) + \int_0^t ds \int d\boldsymbol{p}' W(\boldsymbol{p},\boldsymbol{p}' - e\boldsymbol{E}s)\, f(\boldsymbol{p}' - e\boldsymbol{E}s)\exp\left(-\int_0^t \Gamma_O ds'\right) \tag{2.8}$$

The above equation is the Chamber-Rees path integral [20] and is the form of the Botlzmann equation which can be iteratively solved. In order to make the above equation solvable a useful mathematical trick introduced by Rees [21] is used in which we make the complicated energy dependent function Γ_O into an energy independent term, thereby making the term inside the integral in equation (1.7) trivially solvable. This is done by introducing a scattering term called self-scattering (Γ_{ss}). Self-scattering does not change the momentum or the energy of the particle and therefore does not change the physics of the particle. What this term does however is to convert the energy dependent function Γ_O into an energy independent term by defining

$$\Gamma_{ss}(\mathbf{p}) = \Gamma_T - \Gamma_O(\mathbf{p}) \tag{2.9}$$

Therefore equation (2.8) becomes

$$f(\mathbf{p},t) = f(\mathbf{p},0)e^{-\Gamma_T t} + \int_0^t ds \int d\mathbf{p}' W^*(\mathbf{p},\mathbf{p}' - e\mathbf{E}s) f(\mathbf{p}' - e\mathbf{E}s) e^{-\Gamma_T s} \quad (2.10)$$

where

$$W^*(\mathbf{p},\mathbf{p}') = W(\mathbf{p},\mathbf{p}') + \Gamma_{ss}(\mathbf{p}')\delta(\mathbf{p} - \mathbf{p}') \quad (2.11)$$

The first term of equation (2.10) is a transient term while the second term is the term which can be iteratively solved. If we look at the second term closely the first integral over $d\boldsymbol{p}'$ represents the scattering of the distribution function f out of state $\boldsymbol{p}$ to state ($\boldsymbol{p}' - e\boldsymbol{E}s$). The second integral represents the integration along the trajectory *s* and the exponential is just the probability that no scattering takes place during the time it moves a distance *s*. Thus if we look at how the electrons move physically it consists of a scattering event determined by the first integral and then there is a free-flight motion (no scattering) for a time interval t_s. Rees showed that the time steps t_s correlate to $1/\Gamma_T$. This free-flight scatter sequence is the basis of every Monte-Carlo method used in device simulations.

The Monte Carlo method is mainly used in three different styles, the one-particle Monte Carlo, the ensemble Monte Carlo and the self-consistent ensemble Monte Carlo. In the one-particle Monte Carlo method a single carrier's motion is tracked for a certain period of time till the particle has reached steady state. This method is mostly useful to study bulk properties, like the steady state drift velocity as a function of field.

In the ensemble Monte Carlo method a large ensemble of carriers are simulated at the same time. This method can be sped up using parallelization and

is useful for super-computation. This method is mostly useful for transient analysis as ensemble averages can be taken at certain time steps during the simulation.

In the self-consistent ensemble Monte Carlo method, the ensemble Monte Carlo method is coupled with a Poisson solver or also a Schrödinger solver and is the most suitable method for device simulations.

2.2. Single Particle Monte Carlo Method

As was mentioned earlier there are free flight times (drift times) and then scatter sequences in the Monte Carlo method. If $P[k(t)]dt$ is the probability that an electron in state *k* suffers a collision during the time interval *dt* then the probability that an electron which has had a collision at time t=0 has not yet undergone another collision after time t is [22],

$$P = e^{-\int_0^t P[k(t)]dt} \tag{2.12}$$

Therefore, the probability $P(t)$ that the electron will suffer a collision during dt around t is,

$$P(t)dt = P[k(t)]e^{-\int_0^t P[k(t)]dt}dt \tag{2.13}$$

If Γ_T is the maximum of $P[(k(t)]$ in the region of k-space then,

$$P(t)dt = \Gamma_0 e^{-\Gamma_T t}dt \tag{2.14}$$

Using a random variable transformation and integrating equation (2.14) on both sides we obtain,

$$t_c = -\frac{1}{\Gamma_T}\ln(r) \tag{2.15}$$

where r is a random number between 0 and 1.

As can be seen the value of t_i will have a higher probability of being a value around $1/\Gamma_T$ and if we take a large number of particles the average t_i will be around $1/\Gamma_T$,

$$\int_{0^+}^{1} -\frac{1}{\Gamma_T} ln(x)dx \cong \frac{1}{\Gamma_T} \tag{2.16}$$

The total scattering rate Γ_T is calculated by adding up all the scattering rates of individual types of scattering as well as the self-scattering rate which are all energy dependent.

$$\Gamma_T = \sum_{i=1}^{n} \Gamma_i(E) + \Gamma_{ss}(E) \tag{2.17}$$

where n is the total number of scattering types considered for a particular material (e.g. acoustic phonon scattering, optical phonon scattering etc..) As you can see the value of Γ_T has no upper limit, only a lower limit. It obviously cannot be lower than $\sum_{i=1}^{n} \Gamma_i(E)$. But as $\sum_{i=1}^{n} \Gamma_i(E)$ is energy dependent it is important that Γ_T be greater than $\sum_{i=1}^{n} \Gamma_i(E_s)$ where E_s is the energy of the scattering table at which the cumulative scattering rate is the maximum.

Once the particle has drifted it is time to scatter it. The type of scattering to be used is chosen from the scattering tables. The usual method is to store the

scattering values for each type as a fraction of the total scattering rate Γ_T. The figure below better explains this method.

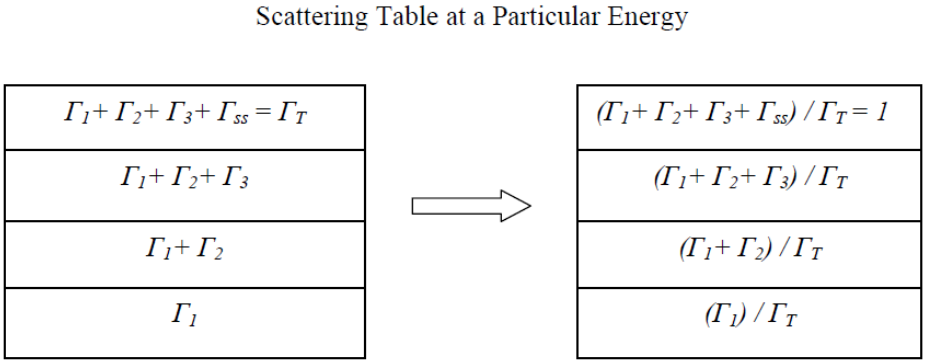

Figure 2.1 Construction of scattering tables (left panel) and scattering tables renormalization (right panel)

A random number (R) is chosen between 0 and 1 and if

$$\sum_{i=0}^{j}\frac{\Gamma_i}{\Gamma_T} < R \leq \sum_{i=0}^{j+1}\frac{\Gamma_i}{\Gamma_T} \quad \text{where } j = 0,1,2,..n \;\&\; \Gamma_{j+1} = \Gamma_{ss} \tag{2.18}$$

Then scattering type $j+1$ is chosen. Here of course $\Gamma_0 = 0$. If self scattering is chosen we do nothing and move on. Once enough time has elapsed, the average carrier velocity is calculated using

$$v_d = \frac{1}{t_{total}}\sum_i \int_{t_{i-1}}^{t_i} v(t)dt \tag{2.19}$$

This average is only valid as long as the distribution function is in steady state. This prevents the analysis of transient behavior like velocity overshoot effects, or

any other non-ergodic process. But using the single particle Monte Carlo method the steady state velocity, energy and other parameters can be calculated.

2.3. Ensemble Monte Carlo Method

A different approach than what is described in the previous section is commonly used by most, and that is the ensemble Monte Carlo Method. Instead of following a single particle for hundreds of thousands of iterations, thousands of particles can be followed for a much lesser number of iterations. In this thesis the ensemble Monte Carlo method is adopted. The time coordinate of each electron must be maintained during the simulation.

The physical quantities such as velocity and energy are averaged over the whole ensemble at frequent time intervals so as to obtain the time evolution of these quantities. For example,

$$v_d(t) = \frac{1}{N}\sum_{i=1}^{N} v_i(t) \quad \text{and} \quad E(t) = \frac{1}{N}\sum_{i=1}^{N} E_i(t) \tag{2.20}$$

where N is the number of particles in the ensemble and t is one of the time intervals at which the ensemble averages are taken. The general block diagram of an ensemble Monte Carlo code is shown in figure 2.2. In figure 2.2 the initial distribution of carriers is a Maxwellian distribution at the given temperature.

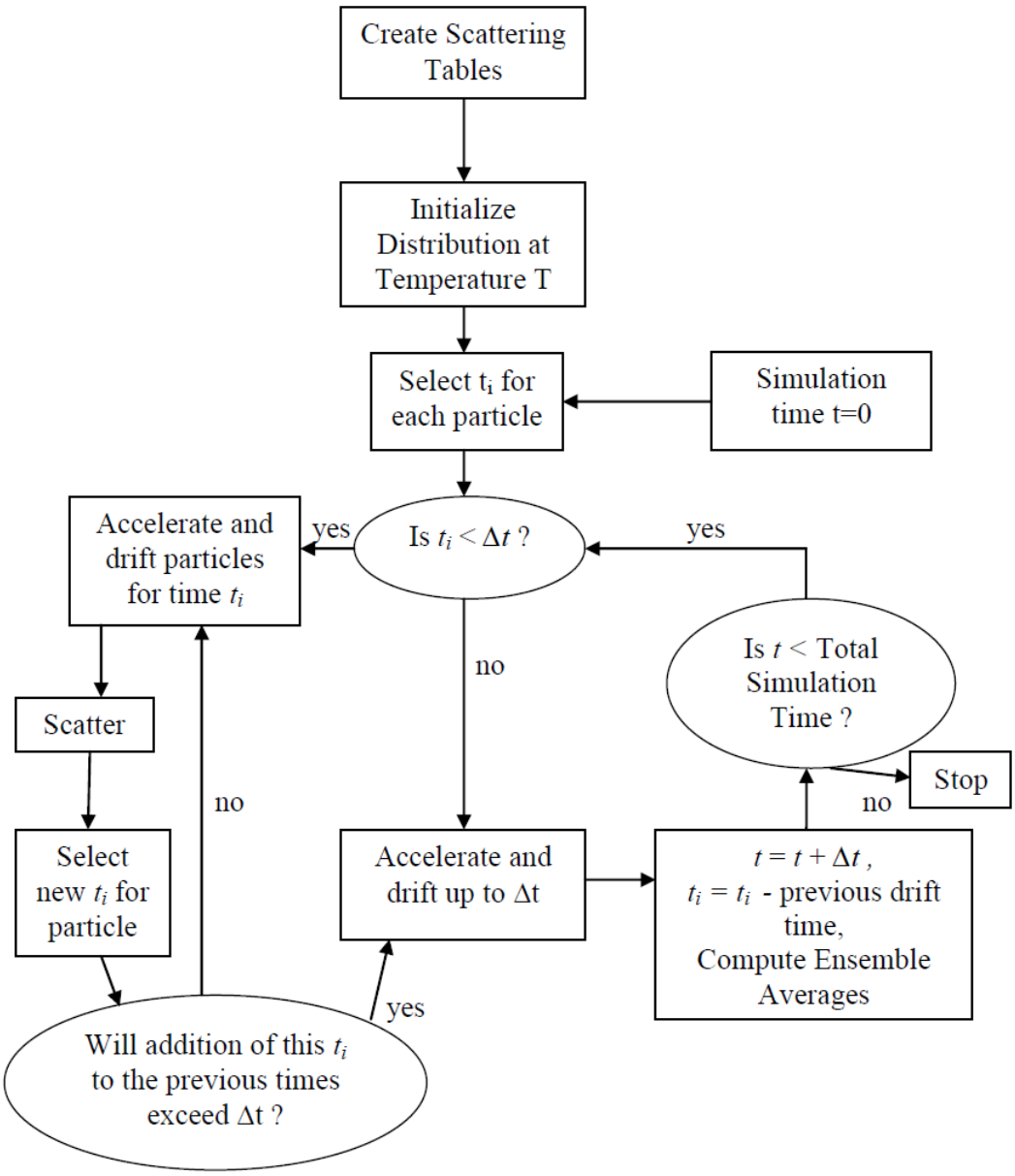

Figure 2.2 Block Diagram of the Ensemble Monte Carlo Code

The ensemble Monte Carlo method does not require steady state conditions to calculate the ensemble averages and therefore can be used to investigate transients in devices. The equation (2.21) and equation (2.22)

represents an estimate of the true velocity and energy which has a standard error of $\frac{\sigma}{\sqrt{N}}$ where σ^2 is the variance that is estimated from [23],

$$\sigma^2 \approx \frac{N}{N-1}\left\{\frac{1}{N}\sum_{j=1}^{N}\left({v_j}^2(t)\right) - v_d(t)^2\right\} \tag{2.21}$$

and

$$\sigma^2 \approx \frac{N}{N-1}\left\{\frac{1}{N}\sum_{j=1}^{N}\left({E_j}^2(t)\right) - E(t)^2\right\} \tag{2.22}$$

for the velocity and energy calculations respectively. Typically the value of N is of the order of 10^4 or 10^5. To obtain the time evolution of certain physical quantities the need to 'freeze' the simulation comes up. The time steps Δt at which the simulation is paused and the ensemble averages taken should not be much larger than the maximum frequency of scattering. If it is it will cause a coarsening of the time evolution and a loss of information. If the time step is too small then it will create noise in the output. Therefore a balance is needed for the time steps. One usually keeps it at a few femtoseconds. Therefore there are two different time scales used in this method, the free-flight duration time and the sampling time. The different time coordinates are shown in the figure below.

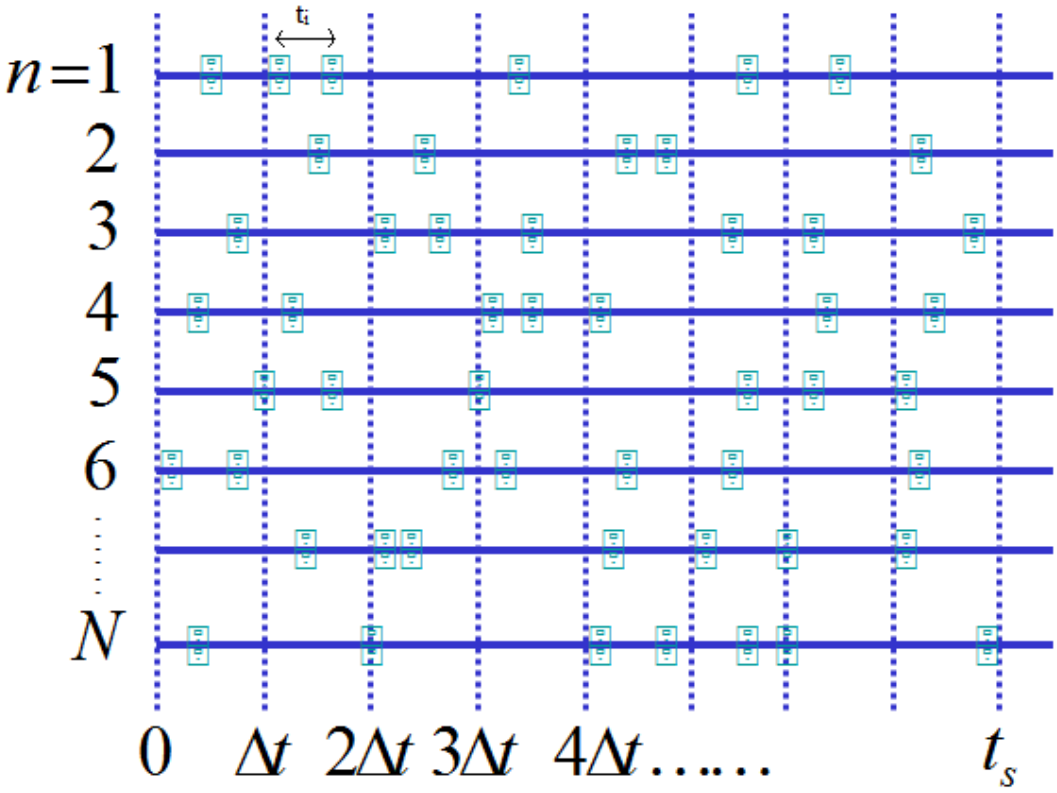

Figure 2.3 Free-Flight Scatter representation of the Monte Carlo Method

In the above figure N is the total number of particles in the simulation while t_s is the total simulation time and t_i is the free-flight duration time for the i^{th} particle. The simulation is paused and the ensemble averages are taken at every Δt as shown in figure 2.3.

2.4. Fermi's Golden Rule

The scattering processes which interrupt the carrier free-flights are calculated quantum mechanically. The scattering event is treated by defining a scattering potential, which is calculated for each type of scattering process. Each of the different processes, or interactions leads to a different "matrix element" form in terms of its dependence on the initial wave vector, the final wave vector and their corresponding energies. The matrix element is given by,

$$M(k,k') = < \psi_{k',q} | H | \psi_{k,q} > \tag{2.23}$$

For three dimensional cases the matrix element usually contains the momentum conservation condition which comes about due to the overlap of the normal Bloch functions of the electrons.

Solving the time-dependent Schrödinger equation using first-order perturbation theory leads to the equation for the scattering rate from a state k to k′ as,

$$P(k,k') = \frac{2\pi}{\hbar} |M(k,k')|^2 \delta(E_k - E_{k'} \pm \hbar\omega_q) \tag{2.24}$$

Equation (2.24) is called Fermi's Golden Rule, where k and k' are the initial and final states of the carrier, E_k and $E_{k'}$ are the corresponding kinetic energies and $\hbar\omega_q$ is the phonon energy and $\delta(E_k - E_{k'} \pm \hbar\omega_q)$ describes the conservation of energy during the scattering process. The conservation of energy is only valid in the long-time limit, i.e. when the scattering events are infrequent. The top sign is for absorption and the bottom sign is for the phonon emission process.

The total scattering rate out of a state defined by wave vector k and the energy E_k is obtained by summing over all k' states in equation (2.24).

$$\Gamma(k) = \frac{2\pi}{\hbar}\sum_{k'}|M(k,k')|^2\delta(E_k - E_{k'} \pm \hbar\omega_q) \tag{2.25}$$

In equation (2.25) the sum over all k' states can be converted to an integral over k' giving,

$$\Gamma(k) = \frac{\Omega}{(2\pi)^3}\int_0^{2\pi} d\phi \int_0^{\pi} sin\theta d\theta \int_0^{\infty} P(k,k')dk' \tag{2.26}$$

where Ω is the total volume of the crystal and $P(k,k')$ is given by equation (2.24). Equation (2.26) is used to calculate scattering rates as a function of energy.

2.5. Non-Parabolic bands

The equation mapping the energy of an electron above the valley minima to its wave vector k using the parabolic band approximation is,

$$E = \frac{\hbar^2 k^2}{2m} \tag{2.27}$$

This approximation is only valid for energies slightly greater than the energy of the valley minima. For Monte Carlo simulations in which high field transport is essential this approximation is not accurate enough. To improve accuracy we need a function that better maps the energy of an electron to its wave vector. A full band calculation will give us a more accurate mapping of energy and momentum of an electron but as it is not an analytic function it becomes hard to switch freely between the energy and momentum which is essential to do in a Monte-Carlo

simulation. Therefore, the full band simulations are very computer intensive. In order to use an analytic approach and still improve upon the accuracy the **k.p** method is used to obtain the non-parabolic equation [24],

$$E(1+\alpha E)=\frac{\hbar^2 k^2}{2m} \tag{2.28}$$

Here α is a term coming from the **k.p** method which depends on the material as,

$$\alpha=\frac{1}{E_g}\left(1-\frac{m_c}{m_0}\right) \tag{2.29}$$

where E_g is the energy difference between the conduction band and the valence band at the Γ point, m_0 is the electron rest mass and m_c is the conductivity mass. The above equation is also an approximation valid as long as,

$$\frac{\hbar^2 k^2}{2m} \ll E_g \tag{2.30}$$

For electron energies in which $\hbar^2 k^2/2m \sim E_g$ the above equation fails and a full band calculation is required to more accurately simulate transport in the material. Assuming that the above assumptions are valid it is important to note the changes that the non-parabolic band approximation introduces. The density of states and the conductivity effective masses are given by,

$$m_d=\hbar^2\left(\frac{\partial^2 E}{\partial k^2}\right)^{-1} \quad \text{and} \quad m_{cm}=\hbar^2 k\left(\frac{\partial E}{\partial k}\right)^{-1} \tag{2.31}$$

For parabolic bands both the masses turn out to be equal to m, but when non-parabolic bands are used we get,

$$m_d = m(1 + 2\alpha E)^3 \quad \text{and} \quad m_{cm} = m(1 + 2\alpha E) \tag{2.32}$$

It is interesting to note that in this method as the electron gains more and more energy its effective mass increases. This means that the electron becomes 'heavier' or reacts slower to the electric field as its energy increases. The change in density of states effective mass causes the scattering rates to get modified slightly as compared to the parabolic bands case. The rest of the chapter deals with the scattering rates commonly used and the formula used to calculate those rates assuming non-parabolic bands.

2.6. Deformation Potential Scattering

Electrons interacting with the vibrations in the crystal lattice give rise to deformation potential scattering. These vibrations stress the lattice producing an elastic strain. When neighboring atoms in a lattice oscillate in the same direction, they give rise to the acoustic branch in the phonon spectra, giving rise to acoustic phonon scattering.

When neighboring atoms oscillate in the opposite direction, they give rise to the optical branch of the phonon spectra, giving rise to non-polar optical phonon scattering.

The essential concept due to Bardeen and Shockley [25] in calculating the deformation potentials is that, if the solid is subject to a strain that is a slowly varying function of position, there will be a change in the energy of the electronic

state that is proportional to the strain. Therefore the Hamiltonian due to the deformation potential electron-phonon interaction is,

$$H_{ep,dp} = c\Delta = c\frac{\delta V}{V} \tag{2.33}$$

where $\frac{\delta V}{V}$ is the strain caused due to the lattice vibrations and c is a deformation potential constant.

2.6.1. Acoustic Phonon Scattering

In order to calculate the scattering rate due to acoustic phonons the 'matrix element' given by equation (2.23) needs to be calculated, which means the Hamiltonian for the electron phonon interaction needs to be calculated. This is given by equation (2.33). In case of acoustic phonons the volume dilation ($\frac{\delta V}{V}$) is given by,

$$\frac{\delta V}{V} = \nabla . \mathbf{u}(\mathbf{r}, t) \tag{2.34}$$

where the operator for the lattice displacement vector $u(\mathbf{r}, t)$, that appears in equation (2.34), is a function of time t and position **r**, and is given by,

$$\mathbf{u}(\mathbf{r}, t) = \sum_{\mathbf{q}} \left(\sqrt{\frac{\hbar}{2\rho\Omega\omega_{\mathbf{q}}}} \right) \mathbf{e}_{\mathbf{q}} \left[a_{\mathbf{q}} + a_{\mathbf{q}}^{+} \right] e^{i\mathbf{q}.\mathbf{r}} \tag{2.35}$$

where $\mathbf{q} = \mathbf{k} - \mathbf{k}'$ is the phonon wave vector, ρ is the density, $\hbar\omega_{\mathbf{q}}$ is the phonon energy, Ω is the crystal volume, $\mathbf{e}_{\mathbf{q}}$ is the unit polarization vector, a_q and a_q^+ are the annihilation and creation of phonon operators.

This gives the Hamiltonian for the interaction to be,

$$H_{ep,dp} = c\Delta = E_{ac}\nabla.\mathbf{u}(\mathbf{r},t) \tag{2.36}$$

where E_{ac} is the acoustic deformation potential constant which is an experimentally determined parameter within certain limits. The final 'matrix element' squared given by equation (2.23) which will be used in equation (2.26) to calculate the scattering rate is,

$$|M(\mathbf{k},\mathbf{k}')|^2 = \frac{\hbar {E_{ac}}^2}{2\rho\Omega\omega_{\mathbf{q}}} q^2 \left(n_{\mathbf{q}} + \frac{1}{2} \mp \frac{1}{2}\right) \delta(\mathbf{k} - \mathbf{k}' \pm \mathbf{q}) \tag{2.37}$$

where $n_{\mathbf{q}}$ is the equilibrium number of phonon in a state $\mathbf{q}$ given by,

$$n_{\mathbf{q}} = \frac{1}{e^{\frac{\hbar\omega_{\mathbf{q}}}{K_B T}} - 1} \tag{2.38}$$

Equation (2.37) is further approximated to simplify the calculation. The first approximation assumes that the acoustic phonon energy is much lesser than the average energy of an electron at lattice temperature T. This means,

$$\hbar\omega_{\mathbf{q}} \ll K_B T \tag{2.39}$$

The elastic approximation also leads to equation (2.38) becoming

$$n_{\mathbf{q}} \approx n_{\mathbf{q}} + 1 \approx \frac{K_B T}{\hbar\omega_{\mathbf{q}}} \gg 1 \tag{2.40}$$

This approximation is called the equipartition approximation and is obviously not valid at low temperatures. Applying this to equation (2.37) we get,

$$|M(\mathbf{k},\mathbf{k}')|^2 = \frac{\hbar {E_{ac}}^2}{2\rho\Omega\omega_{\mathbf{q}}} q^2 \left(\frac{K_B T}{\hbar\omega_{\mathbf{q}}}\right) \delta(\mathbf{k} - \mathbf{k}' \pm \mathbf{q}) \tag{2.41}$$

The second approximation is to assume that the dispersion relation of acoustic phonons is linear (Debye limit). This means that,

$$\omega_{\mathbf{q}} = v_s q \tag{2.42}$$

where v_s is the velocity of sound in the crystal.

This as can be seen in figure 2.9 is a reasonable approximation for low energies near the gamma point. This approximation further simplifies equation (2.41) to,

$$|M(\mathbf{k},\mathbf{k}')|^2 = \frac{{E_{ac}}^2 K_B T}{\rho \Omega v_s^2} \delta(\mathbf{k} - \mathbf{k}' \pm \mathbf{q}) \tag{2.43}$$

This expression is then substituted into equation (2.24) and the scattering rate is calculated as a function of energy using the method given in section 2.4. The final expression of acoustic phonon scattering rate obtained using a non-parabolic band structure is,

$$W(E) = \left(\frac{2\pi {E_{ac}}^2 K_B T}{\rho \hbar v_s^2}\right)\left(\frac{(2m)^{3/2}\sqrt{E(1+\alpha E)}}{4\pi^2 \hbar^3}\right)(1+2\alpha E) \tag{2.44}$$

2.6.2. Non-Polar Optical Phonon Scattering

To calculate the scattering rate due to non-polar optical phonons, a similar method to that used previously has to be employed. This means the Hamiltonian for the electron phonon interaction needs to be calculated. In the case of optical phonons the neighboring atoms oscillate in the opposite direction, thus directly affecting the size of the unit cell. Because of this, the volume dilation ($\frac{\delta V}{V}$) is given by,

$$\frac{\delta V}{V} = \mathbf{u}(\mathbf{r}, t) \tag{2.45}$$

This gives the Hamiltonian for the interaction to be,

$$H_{ep,dp} = c\Delta = D_{iv}\mathbf{u}(\mathbf{r}, t) \tag{2.46}$$

where D_{iv} is the optical deformation potential constant which is an experimentally determined parameter within certain limits. The operator for the lattice displacement vector $u(\mathbf{r}, t)$ is given by equation (2.35). The final 'matrix element' squared given by equation (2.23) which will be used in equation (2.24) to calculate the scattering rate then becomes,

$$|M(\mathbf{k}, \mathbf{k}')|^2 = \frac{\hbar {D_{iv}}^2}{2\rho\Omega\omega_{\mathbf{q}}}\left(n_{\mathbf{q}} + \frac{1}{2} \mp \frac{1}{2}\right)\delta(\mathbf{k} - \mathbf{k}' \pm \mathbf{q}) \tag{2.47}$$

where $n_{\mathbf{q}}$ is the number of phonon in a state $\mathbf{q}$ given by equation (2.38).

An approximation used here to simply calculations is that $\omega_{\mathbf{q}} = \omega_0$ for optical phonons (Einstein model). This basically means that the optical phonons are dispersionless, this is a reasonable approximation when you look at figure 2.9. This approximation reduces equation (2.47) to,

$$|M(\mathbf{k}, \mathbf{k}')|^2 = \frac{\hbar {D_{iv}}^2}{2\rho\Omega\omega_0}\left(n_0 + \frac{1}{2} \mp \frac{1}{2}\right)\delta(\mathbf{k} - \mathbf{k}' \pm \mathbf{q}) \tag{2.48}$$

This expression is then substituted into equation (2.24) and the scattering rate is calculated as a function of energy using the method given in section 2.4. The final expression of optical phonon scattering rate (intervalley scattering) from valley i to valley j obtained using a non-parabolic band structure is,

$$W(E)=\left(\frac{\pi D_{ij}^2 Z_j}{\rho\omega_{ij}}\right)*\left(n(\omega_{ij})+\frac{1}{2}\mp\frac{1}{2}\right)*\left(\frac{(2m_d)^{3/2}\sqrt{E_f(1+\alpha E_f)}}{4\pi^2\hbar^3}\right)*(1+2\alpha E_f) \tag{2.49}$$

$$n(\omega_{ij})=\frac{1}{e^{\frac{\hbar\omega_{ij}}{K_B T_L}}-1} \tag{2.50}$$

$$E_f = E\pm\hbar\omega_{ij}-\Delta E_{ij} \tag{2.51}$$

D_{ij} is the deformation potential for transition from valley i to valley j, ρ is the density of the material and Z_f is the number of final valleys to scatter into.

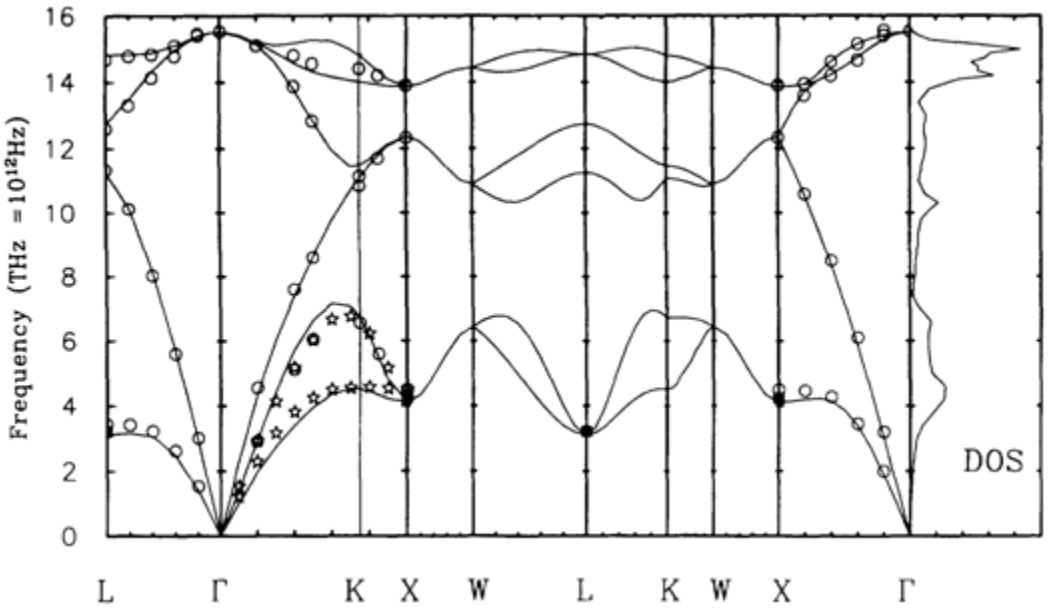

Figure 2.4 The phonon dispersion relation in bulk silicon using the valence force field model

For intervalley processes the interaction described by equation (2.46) is the zeroth order interaction. Ferry [26] considered the first order interaction process, for which the matrix element is,

$$|M(\mathbf{k},\mathbf{k}')|^2 = \frac{\hbar {D_{1iv}}^2 q^2}{2\rho\Omega\omega_0}\left(n_0 + \frac{1}{2} \mp \frac{1}{2}\right)\delta(\mathbf{k}-\mathbf{k}' \pm \mathbf{q}) \tag{2.52}$$

which gives the total scattering rate out of state **k** as,

$$W(E) = \frac{\sqrt{2}m^{\frac{5}{2}}{D_{1iv}}^2}{\pi\rho\omega_0\hbar^5}\left(n_0 + \frac{1}{2} \mp \frac{1}{2}\right)G(E) \tag{2.53}$$

where

$$G(E) = \sqrt{E_f(1+\alpha E_f)}(1+2\alpha E_f)\left[E(1+\alpha E) + E_f(1+\alpha E_f)\right] \tag{2.54}$$

2.7. Polar Optical Phonon Scattering

In polar materials there is an atom with charge greater than four and an atom with charge less than four. This imbalance causes a net electronic charge transfer from the atom with greater charge to the atom with lesser charge. For covalent bonds in which the electrons are shared between different bonding orbitals there is only a fractional charge transfer given by the 'effective charge', e^*. This small charge transfer leads to an effective dipole, which leads to a finite ionic contribution to the dielectric function.

The lattice vibrations of the crystal cause this dipole to oscillate creating a scattering potential. The electron-phonon interaction is described by the Fröhlich Hamiltonian which, including screening of electrons is given by [27],

$$H_{ep}(r) = \sum_{\mathbf{q}} \frac{iee^*}{\varepsilon_\infty \Omega}\left(\frac{q}{q^2+q_d^2}\right)\sqrt{\frac{\hbar}{2M^* N_u \omega_{\mathbf{q}}}}\left[a_{\mathbf{q}} e^{i\mathbf{q}.\mathbf{r}} + a_{\mathbf{q}}^{+} e^{-i\mathbf{q}.\mathbf{r}}\right] \tag{2.55}$$

where N_u is the number of atoms in a unit cell. The effective charge e^* is given by,

$$e^{*2} = M^* \Omega \omega_{LO}^2 {\varepsilon_\infty}^2 \left(\frac{1}{\varepsilon_\infty} - \frac{1}{\varepsilon(0)}\right) \tag{2.56}$$

the reduced mass M^* is given by,

$$M^* = \frac{M_1 M_2}{M_1 + M_2} \tag{2.57}$$

and,

$$q_d = \sqrt{\frac{e^2(n+p)}{\varepsilon K_B T}} \tag{2.58}$$

The final 'matrix element' squared given by equation (2.23) which will be used in equation (2.24) to calculate the scattering rate then becomes,

$$|M(\mathbf{k},\mathbf{k}')|^2 = \frac{\hbar e^2 \omega_{LO}}{2\Omega}\left(\frac{q}{q^2+q_d^2}\right)^2 \left(\frac{1}{\varepsilon_\infty} - \frac{1}{\varepsilon(0)}\right)\left(n_0 + \frac{1}{2} \mp \frac{1}{2}\right)\delta(\mathbf{k} - \mathbf{k}' \pm \mathbf{q}) \tag{2.59}$$

Equation (2.55) was simplified by assuming that $\omega_{\mathbf{q}} = \omega_{LO}$ in equation (2.52) for all optical phonons. This expression is then substituted into equation (2.24) and the scattering rate is calculated as a function of energy using the method given in section 2.4. The final expression of polar optical phonon scattering is,

$$W(E) = \frac{\sqrt{m} e^2 \omega_{LO}}{4\sqrt{2}\pi\hbar}\left(\frac{1}{\varepsilon_\infty} - \frac{1}{\varepsilon(0)}\right)\left(n_0 + \frac{1}{2} \mp \frac{1}{2}\right)\left(\frac{1+2\alpha E_f}{\sqrt{\gamma}}\right)\left(G + \frac{q_d^2}{2} H\right) \tag{2.60}$$

where

$$E_f = E \pm \hbar\omega_{LO}$$

$$\gamma = E(1 + \alpha E)$$

$$G = \frac{1}{2} log\left(\frac{\gamma + \gamma_f + 2\sqrt{\gamma_f \gamma} + E_{debye}}{\gamma + \gamma_f - 2\sqrt{\gamma_f \gamma} + E_{debye}}\right)$$

$$\gamma_f = E_f(1 + \alpha E_f)$$

$$E_{debye} = \frac{\hbar^2 q_d^2}{2m} \tag{2.61}$$

$$H = \frac{-4\sqrt{\gamma_f \gamma}}{\left(\hbar\omega_{LO} + E_{debye}\right)^2 + 4\gamma E_{debye}}$$

2.8. Piezoelectric Scattering

In polar materials the charge transfer between two atoms creates long-range macroscopic electric fields which interact with electrons to create a scattering potential. Due to the acoustic modes of phonons, the strain in the lattice changes the electric field and creates a new form of scattering called piezoelectric scattering. The Hamiltonian for this interaction is given by,

$$H_{ep}(r) = -\sum_{\mathbf{q}} \frac{e e_{pz}}{\varepsilon_\infty} \sqrt{\frac{\hbar}{2M^* N_u \omega_{\mathbf{q}}}} \left[a_{\mathbf{q}} e^{i\mathbf{q}.\mathbf{r}} + a_{\mathbf{q}}^+ e^{-i\mathbf{q}.\mathbf{r}}\right] \tag{2.62}$$

This leads to the following expression for the matrix element squared for this scattering mechanism,

$$|M(\mathbf{k},\mathbf{k}')|^2 = \frac{\hbar}{2\rho\Omega\omega_{\mathbf{q}}}\left(\frac{ee_{pz}}{\varepsilon_\infty}\right)^2\left(n_{\mathbf{q}}+\frac{1}{2}\mp\frac{1}{2}\right)\delta(\mathbf{k}-\mathbf{k}'\pm\mathbf{q}) \tag{2.63}$$

Assuming the same approximations as those used in acoustic phonon scattering, namely equipartition approximation and linear dispersion of acoustic phonons we obtain the following relation for the matrix element squared,

$$|M(\mathbf{k},\mathbf{k}')|^2 = \frac{K_B T}{\rho\Omega v_s^2}\left(\frac{q}{q^2+q_d^2}\right)^2\left(\frac{ee_{pz}}{\varepsilon_\infty}\right)^2\delta(\mathbf{k}-\mathbf{k}'\pm\mathbf{q}) \tag{2.64}$$

This expression is then substituted into equation (2.24) and the scattering rate is calculated as a function of energy using the method given in section 2.4. The final expression of piezoelectric scattering is,

$$\mathrm{W(E)} = \left(\frac{\sqrt{2}m_d^{3/2}\mathrm{K_B T_L}}{\pi\rho v_s^2\hbar^4}\right)*\left(\frac{ee_{pz}}{\varepsilon_\infty}\right)^2*\left(\sqrt{E(1+\alpha E)}*(1+2\alpha E)\right)*\left(\frac{1}{q_D^2\left(q_D^2+\frac{8m_d E(1+\alpha E)}{\hbar^2}\right)}\right) \tag{2.65}$$

where v_s is the velocity of sound in the material, e_{pz} is the piezoelectric coupling constant and e_∞ is the high frequency dielectric constant. $q_D$is given by equation (2.58).

2.9. Ionized Impurity Scattering

Ionized impurity scattering occurs as the name suggests due to the deflection of an electron by a Coulomb potential due to ionized impurities. This is an elastic scattering process and is non-isotropic. The scattering rate due to ionized impurities obtained using the Brooks-Herring formula for non-parabolic bands is,

$$W(E)=\left(\frac{\sqrt{2}e^4 N_I {m_d}^{3/2}}{\pi\varepsilon_s^2\hbar^4}\right)*\left(\sqrt{E(1+\alpha E)}*(1+2\alpha E)\right)*\left(\frac{1}{q_D^2\left(q_D^2+\frac{8m_d E(1+\alpha E)}{\hbar^2}\right)}\right) \quad (2.66)$$

N_I is the ionized impurity concentration.

The above scattering rates have all been calculated from their respective matrix elements and the Fermi golden rule under the non-parabolic bands approximation.

2.10. Final Angle after Scattering

An important calculation required is to calculate the final angle after a scattering takes place. A scattering process is anything that changes the momentum of the electron. Certain processes are anisotropic by which we mean they preferably choose certain angles depending on the energy of the electron while others are isotropic which means they have equal probability to scatter the electron in any angle. A useful formula to calculate the final angles after scattering for a certain type of scattering process is [28]

$$\int_0^r dr=\int_0^\phi \frac{d\phi\int_0^\infty\int_0^\pi S\left(\mathbf{p},\mathbf{p}'\right)sin\theta d\theta p'^2 dp'}{\int_0^{2\pi}d\phi\int_0^\infty\int_0^\pi S\left(\mathbf{p},\mathbf{p}'\right)sin\theta d\theta p'^2 dp'} \quad (2.67)$$

and

$$\int_0^r dr=\int_0^\theta \frac{sin\theta d\theta\int_0^\infty\int_0^\pi S\left(\mathbf{p},\mathbf{p}'\right)d\phi p'^2 dp'}{\int_0^{2\pi}\int_0^\infty\int_0^\pi S\left(\mathbf{p},\mathbf{p}'\right)sin\theta d\theta d\phi p'^2 dp'} \quad (2.68)$$

In spherical coordinates all that is required to completely define the coordinates of the final momentum state is $'$, θ and ϕ. k' is obtained based on the final energy after scattering by the formula,

$$k' = \sqrt{\frac{2m_d E_f\left(1+\alpha E_f\right)}{\hbar^2}} \tag{2.69}$$

while θ is determined by equation (2.68) and ϕ is determined by equation (2.67).

Here $S(\boldsymbol{p},\boldsymbol{p}')$ is the matrix element squared for each scattering type. This is in the same form used in the Fermi's golden rule. As all scattering processes have matrix elements independent of ϕ equation (2.67) can be reduced to,

$$\begin{aligned} \int_0^r dr &= \int_0^\phi \frac{d\phi}{2\pi} \\ \Rightarrow \phi &= 2\pi r \end{aligned} \tag{2.70}$$

where r is a random number between 0 and 1.

Final Angles for Isotropic Scattering Processes

For isotropic scattering processes like acoustic phonon scattering, non-polar optical phonon scattering the matrix element is independent of θ. Therefore equation (2.68) can be reduced to,

$$\begin{aligned} \int_0^r dr &= \int_0^\theta \frac{sin\theta d\theta}{2} \\ \Rightarrow cos\theta &= 1-2r \end{aligned} \tag{2.71}$$

where r is a random number between 0 and 1.

Final Angles for Anisotropic Scattering Processes

The non-isotropic scattering processes are ionized impurity scattering, polar optical scattering and piezoelectric scattering. Ionized impurity and piezoelectric scattering have the same relationship with θ so for both processes we can calculate the final angle using,

$$cos\theta = 1 - \frac{2r}{1 + z(1-r)}$$
$$z = \frac{8m_d E(1+\alpha E)}{\hbar^2 q_D^2} \tag{2.72}$$

where *r* is a random number between 0 and 1.

For polar optical scattering the final angle is calculated using,

$$\cos(\theta) = \frac{(1+z) - (1+2z)^r}{z}$$
$$z = \frac{2\sqrt{E(1+\alpha E)(E(1+\alpha E) \pm \hbar\omega_{LO})}}{\sqrt{E(1+\alpha E)} - \sqrt{E(1+\alpha E)(E(1+\alpha E) \pm \hbar\omega_{LO})}} \tag{2.73}$$

where *r* is a random number between 0 and 1.

CHAPTER 3. THE GENERALIZED MONTE CARLO CODE

3.1. Introduction

The purpose of the generalized Monte Carlo code is to give users the option of defining their own material or modifying the definition of an existing material. Technically any number of different materials can be simulated within the non-parabolic band approximation. This makes the code very versatile and necessitates a very general method of implementing the code which results in a large set of input parameters which in turn increases the complexity of the code.

3.2. Input Parameters

In the generalized Monte Carlo code there is a wide range of input parameters. The input parameters are either loaded from a file or from the Rappture interface discussed in Chapter 5. In order to be able to define a material the user can input the number of valleys to be used in the simulation, the number of sub-valleys (equivalent valleys) within each valley, the direction of those sub-valleys, the effective masses of electrons in those sub-valley directions and the energy difference between the bottom of the valleys. In addition to choosing deformation potential scattering (acoustic and optical), ionized impurity scattering, polar-optical phonon scattering and piezoelectric scattering the user can also specify whether the optical phonon scattering within a valley are

umklapp processes like it is needed in Silicon for the case of g-phonon intervalley scattering.

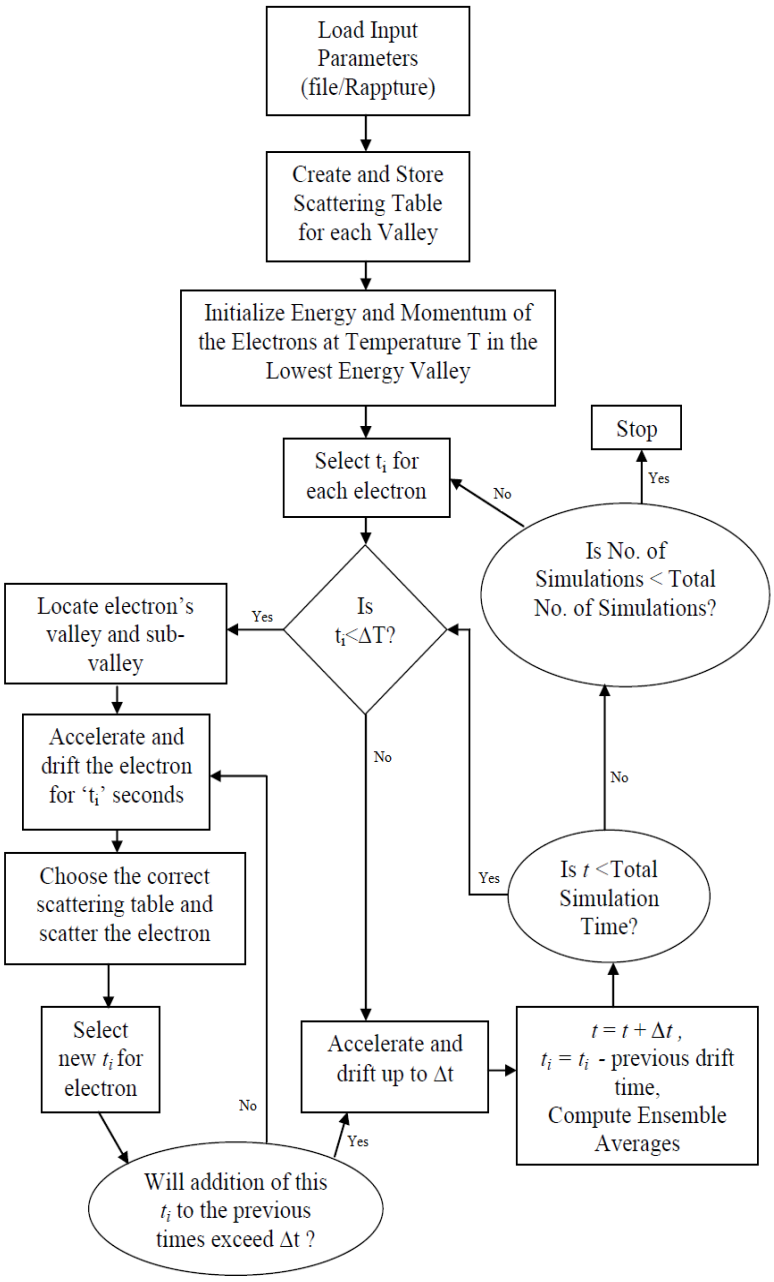

Figure 3.1 Flow chart for the generalized Monte Carlo code

3.3. Creating Scattering Tables

The scattering table has to be created and stored separately for each valley as the scattering parameters depend on the effective mass of the electron which differs from valley to valley. Also some scattering processes might exist in one valley but not in the other for e.g. in Germanium f and g type scattering is considered in the X valley but not in the L valley. Therefore the number of scattering processes can also vary from one valley to another. The scattering tables are normalized to the maximum value of the total scattering rate within the energy range specified by the user which will be different for different valleys.

3.4. Initializing Electrons

The electrons are initialized to a Maxwell distribution at the temperature T. The formulae used to initialize the electron's energy and momentum are,

$$E = \frac{3}{2} K_B T ln\left(\frac{1}{r}\right) \quad 0 < r \leq 1$$

$$k = \sqrt{\frac{2mE(1+\alpha E)}{\hbar^2}}$$

$$k_x = k\sqrt{1-(1-2r)^2}\cos(2\pi r) \tag{3.1}$$

$$k_y = k\sqrt{1-(1-2r)^2}\sin(2\pi r)$$

$$k_z = k(1-2r) \quad 0 \leq r \leq 1$$

The electrons, whose number is defined by the user, are initially placed in the lowest energy valley which is also defined by the user and is equally distributed to

all the sub-valleys present in that valley. Here m is the drift (conductivity) effective mass used to make the bands isotropic.

3.5. Carrier Free-Flights

In between scattering events the electron is drifted under the applied electric field. The equation describing the dispersion relation of the electron for a general sub-valley for non-parabolic bands is,

$$E(1+\alpha E) = \frac{\hbar^2 k_1^2}{2m_1} + \frac{\hbar^2 k_2^2}{2m_2} + \frac{\hbar^2 k_3^2}{2m_3} \tag{3.2}$$

where k_1, k_2, k_3 are the wave-vectors along the three mutually perpendicular directions that define the sub-valley and m_1, m_2, m_3 are the effective masses of the electrons along those directions.

Equation (3.2) represents the dispersion relation for an anisotropic band, which is the most general case. To calculate the drift velocity equations, equation (3.2) must first be converted to an isotropic dispersion relation by changing the wave-vectors $k_1, k_2 \; and \; k_3$ to $k_1', k_2' \; and \; k_3'$ where,

$$k_i' = \sqrt{\frac{m}{m_i}} k_i \qquad i = 1,2,3 \tag{3.3}$$

here m is the conductivity effective mass used for all $k_1', k_2' \; and \; k_3'$. Substituting equation (3.3) into equation (3.2) we get,

$$E(1+\alpha E) = \frac{\hbar^2 (k_1'^2 + k_2'^2 + k_3'^2)}{2m} \tag{3.4}$$

The above equation now represents the dispersion relation of an electron for a spherical band with effective mass m in all directions. According to Newton's second law of motion - the rate of change of momentum is equal to the force applied to the electron giving,

$$\begin{aligned} \Delta\hbar k_1 &= -qE_1 t \\ \Delta\hbar k_2 &= -qE_2 t \\ \Delta\hbar k_3 &= -qE_3 t \end{aligned} \tag{3.5}$$

where $E_1, E_2\ and\ E_3$ are the electric field magnitudes along the mutually perpendicular directions that define the sub-valley. t is the drift time selected by equation (2.15). Substituting equation (3.5) into (3.6) we get,

$$\begin{aligned} k_1' &= k_1' - \frac{qE_1 t}{\hbar} * \sqrt{\frac{m}{m_1}} \\ k_2' &= k_2' - \frac{qE_2 t}{\hbar} * \sqrt{\frac{m}{m_2}} \\ k_3' &= k_3' - \frac{qE_3 t}{\hbar} * \sqrt{\frac{m}{m_3}} \end{aligned} \tag{3.6}$$

The electric field applied to the device is defined by the user before the simulation starts along the (x,y,z) coordinate system. In order to drift the electron according to equation (3.6) we need the electric field magnitudes along the three mutually perpendicular directions (1,2,3) which define the sub-valley in k-space. In general the coordinate system (1,2,3) is completely different from the (x,y,z) coordinate system. Therefore before every electron is drifted, the sub-valley in which the

electron currently exists is identified and the coordinate system is transformed from the (x,y,z) system to the (1,2,3) system which defines that sub-valley in k-space. The electric field acting on the electron is then given by,

$$E_{[a_1b_1c_1]} = \frac{E_x a_1}{\sqrt{(a_1^2+b_1^2+c_1^2)}} + \frac{E_y b_1}{\sqrt{(a_1^2+b_1^2+c_1^2)}} + \frac{E_z c_1}{\sqrt{(a_1^2+b_1^2+c_1^2)}}$$

$$E_{[a_2b_2c_2]} = \frac{E_x a_2}{\sqrt{(a_2^2+b_2^2+c_2^2)}} + \frac{E_y b_2}{\sqrt{(a_2^2+b_2^2+c_2^2)}} + \frac{E_z c_2}{\sqrt{(a_2^2+b_2^2+c_2^2)}} \qquad (3.7)$$

$$E_{[a_3b_3c_3]} = \frac{E_x a_3}{\sqrt{(a_3^2+b_3^2+c_3^2)}} + \frac{E_y b_3}{\sqrt{(a_3^2+b_3^2+c_3^2)}} + \frac{E_z c_3}{\sqrt{(a_3^2+b_3^2+c_3^2)}}$$

where the three mutually perpendicular directions that describe the sub-valley are $[a_1,b_1,c_1]$, $[a_2,b_2,c_2]$ and $[a_3,b_3,c_3]$. According to equation (3.6) we also need to have the wave vectors along the directions $[a_1,b_1,c_1]$, $[a_2,b_2,c_2]$ and $[a_3,b_3,c_3]$. This is obtained by doing another transformation which gives,

$$k_{[a_1b_1c_1]} = \frac{k_x a_1}{\sqrt{(a_1^2+b_1^2+c_1^2)}} + \frac{k_y b_1}{\sqrt{(a_1^2+b_1^2+c_1^2)}} + \frac{k_z c_1}{\sqrt{(a_1^2+b_1^2+c_1^2)}}$$

$$k_{[a_2b_2c_2]} = \frac{k_x a_2}{\sqrt{(a_2^2+b_2^2+c_2^2)}} + \frac{k_y b_2}{\sqrt{(a_2^2+b_2^2+c_2^2)}} + \frac{k_z c_2}{\sqrt{(a_2^2+b_2^2+c_2^2)}} \qquad (3.8)$$

$$k_{[a_1b_1c_1]} = \frac{k_x a_3}{\sqrt{(a_3^2+b_3^2+c_3^2)}} + \frac{k_y b_3}{\sqrt{(a_3^2+b_3^2+c_3^2)}} + \frac{k_z a_3}{\sqrt{(a_3^2+b_3^2+c_3^2)}}$$

The electron is then drifted according to equation (3.6) and the coordinates system is transformed back to the (x,y,z) coordinate system using,

$$k_x = \frac{a_1 k_{[a_1 b_1 c_1]}}{\sqrt{(a_1^2 + b_1^2 + c_1^2)}} + \frac{a_2 k_{[a_2 b_2 c_2]}}{\sqrt{(a_2^2 + b_2^2 + c_2^2)}} + \frac{a_3 k_{[a_3 b_3 c_3]}}{\sqrt{(a_3^2 + b_3^2 + c_3^2)}}$$

$$k_y = \frac{b_1 k_{[a_1 b_1 c_1]}}{\sqrt{(a_1^2 + b_1^2 + c_1^2)}} + \frac{b_2 k_{[a_2 b_2 c_2]}}{\sqrt{(a_2^2 + b_2^2 + c_2^2)}} + \frac{b_3 k_{[a_3 b_3 c_3]}}{\sqrt{(a_3^2 + b_3^2 + c_3^2)}} \quad (3.9)$$

$$k_z = \frac{c_1 k_{[a_1 b_1 c_1]}}{\sqrt{(a_1^2 + b_1^2 + c_1^2)}} + \frac{c_2 k_{[a_2 b_2 c_2]}}{\sqrt{(a_2^2 + b_2^2 + c_2^2)}} + \frac{c_3 k_{[a_3 b_3 c_3]}}{\sqrt{(a_3^2 + b_3^2 + c_3^2)}}$$

The energy of the electron is then calculated by using,

$$Energy = \frac{G}{1 + \sqrt{1 + 2\alpha G}} \quad (3.10)$$

where

$$G = \frac{\hbar^2 ({k_x}^2 + {k_y}^2 + {k_z}^2)}{m} \quad (3.11)$$

where m is the mass used in equation (3.3) to make the sub-valley spherically symmetric. Therefore whenever a change from energy to momentum or vice-versa is required the mass m for that particular sub-valley must be used. In this code the mass m is always the 'drift (conductivity) mass' of the sub-valley or,

$$\frac{3}{m} = \frac{1}{m_1} + \frac{1}{m_2} + \frac{1}{m_3} \quad (3.12)$$

where $m_1, m_2 \; and \; m_3$ are the effective masses of the electron along the three mutually perpendicular directions that define the sub-valley.

3.6. Scattering the Electron

The scattering type is chosen by the method mentioned in the previous chapter. It would depend on the valley the electron is in at the time the scattering

takes place as the scattering tables are different for different valleys. Therefore it is necessary to keep track of which valley and which sub-valley the electron is in at all times. If the scattering type chosen is non-polar optical phonon scattering from valley 1 to valley 2 then the final sub-valley of the electron is randomly chosen from all the sub-valleys present in valley 2 as they are all at the same energy level and should therefore have equal probability of being scattered into. If there is non-polar optical phonon scattering within a valley then the final sub-valley of the electron will depend on whether f and g type scattering occurs or not. If there isn't any f and g type scattering then the final sub-valley is randomly chosen from the remaining sub-valleys in that valley. If f and g type scattering is present and if the f-type scattering process is chosen then the final sub-valley is randomly chosen from all remaining sub-valleys in the valley which are not in the same axis as the present sub-valley. In the case of g-type scattering the final sub-valley is the other sub-valley which lies on the same axis as the present sub-valley.

3.7. Calculating Ensemble Averages

At the end of every time step the ensemble averages are calculated. This involves calculating the average drift velocity of the electrons, the average energy of the electrons and the number of electrons present in each valley and sub-valley. The average energy is calculated using,

$$\langle E \rangle = \frac{1}{N}\sum_{i=1}^{N} E_i \tag{3.13}$$

where E_i is the energy of the i[th] electron. The average energies within a sub-valley 'j' in valley 'i' is,

$$\langle E_{i,j} \rangle = \frac{1}{N_{i,j}}\sum_{k=1}^{N_{i,j}} E_{i,j,k} \tag{3.14}$$

where $E_{i,j,k}$ is the energy of the k[th] electron in the j[th] sub-valley of the i[th] valley and $N_{i,j}$ is the number of electrons in the j[th] sub-valley of the i[th] valley.

Calculation of drift velocity in many valley semiconductors

In most semiconductors in order to properly simulate high field transport it is necessary to consider more than 1 conduction band valley. To calculate the drift velocity along any direction the effective mass along that particular direction is required. This makes it a little complicated to calculate the average drift velocity as different valleys are orientated differently in k-space and we only have the effective mass values along specific directions within each sub-valley. For example, in GaAs a sub-valley of the L valley lies along the [111] direction. We know the effective masses along the transverse and longitudinal directions of the sub-valley but we do not know the effective mass along the [100] direction of that sub-valley. In order to calculate the drift velocity along the [100] direction we transform the coordinate system to a system along which we know the effective masses and then switch back to the original coordinate system.

Assume the Monte-Carlo simulation is run on the x,y and z coordinate system where the x-direction is [100] , y-direction is [010] and z-direction is [001]. Each sub-valley can be completely described by three mutually perpendicular axes. Let the three mutually perpendicular directions that describe the sub-valley be $[a_1,b_1,c_1]$, $[a_2,b_2,c_2]$ and $[a_3,b_3,c_3]$. The electrons in the Monte-Carlo simulation will be drifted according to the x,y and z coordinate system so there will be k_x , the component of the wave vector along [100], k_y , the component of the wave vector along [010] and k_z , the component of the wave vector along [001]. Therefore the total wave vector of the electron can be written as,

$$\boldsymbol{k} = k_x\hat{\boldsymbol{\imath}} + k_y\hat{\boldsymbol{\jmath}} + k_z\hat{\boldsymbol{z}} \tag{3.15}$$

The drift velocity along $[a_1,b_1,c_1]$ under the non-parabolic band approximation is calculated using,

$$v_{drift} = \frac{1}{\hbar}\frac{\partial E(k)}{\partial k} \tag{3.16}$$

where $E(k)$ is the electron dispersion relation for the electrons in the valley. Equation (3.16) is valid only for spherical valleys, therefore we have to convert the anisotropic valley to an isotropic valley by using the method described earlier. After making the valley isotropic the drift velocity is,

$$v_{d,[a_1b_1c_1]} = \frac{\hbar k_{[a_1b_1c_1]}}{\sqrt{m * m_{[a_1b_1c_1]}}(1 + 2\alpha E)} \tag{3.17}$$

where $k_{[a_1b_1c_1]}$ is the component of the wave vector along [a_1,b_1,c_1] and $m_{[a_1b_1c_1]}$ is the effective mass of the electron along [a_1,b_1,c_1], m is the conductivity effective mass used to make the valley isotropic in equation (3.3) and E is the energy of the electron in that valley. Similarly the drift velocity along [a_2,b_2,c_2] and [a_3,b_3,c_3] is given by,

$$v_{d,[a_2b_2c_2]} = \frac{\hbar k_{[a_2b_2c_2]}}{\sqrt{m * m_{[a_2b_2c_2]}}(1+2\alpha E)}$$
$$v_{d,[a_3b_3c_3]} = \frac{\hbar k_{[a_3b_3c_3]}}{\sqrt{m * m_{[a_3b_3c_3]}}(1+2\alpha E)} \quad (3.18)$$

Using a simple transformation of coordinates from x,y and z coordinate system to the [a_1,b_1,c_1], [a_2,b_2,c_2] and [a_3,b_3,c_3] coordinate system we get,

$$k_{[a_1b_1c_1]} = \frac{k_x a_1}{\sqrt{(a_1^2+b_1^2+c_1^2)}} + \frac{k_y b_1}{\sqrt{(a_1^2+b_1^2+c_1^2)}} + \frac{k_z c_1}{\sqrt{(a_1^2+b_1^2+c_1^2)}}$$
$$k_{[a_2b_2c_2]} = \frac{k_x a_2}{\sqrt{(a_2^2+b_2^2+c_2^2)}} + \frac{k_y b_2}{\sqrt{(a_2^2+b_2^2+c_2^2)}} + \frac{k_z c_2}{\sqrt{(a_2^2+b_2^2+c_2^2)}} \quad (3.19)$$
$$k_{[a_1b_1c_1]} = \frac{k_x a_3}{\sqrt{(a_3^2+b_3^2+c_3^2)}} + \frac{k_y b_3}{\sqrt{(a_3^2+b_3^2+c_3^2)}} + \frac{k_z a_3}{\sqrt{(a_3^2+b_3^2+c_3^2)}}$$

The coordinates system is then transformed once again back to the x,y and z coordinate system to get the drift velocities along the x,y and z directions.

$$v_x = \frac{a_1 v_{d,[a_1 b_1 c_1]}}{\sqrt{(a_1^2 + b_1^2 + c_1^2)}} + \frac{a_2 v_{d,[a_2 b_2 c_2]}}{\sqrt{(a_2^2 + b_2^2 + c_2^2)}} + \frac{a_3 v_{d,[a_3 b_3 c_3]}}{\sqrt{(a_3^2 + b_3^2 + c_3^2)}}$$

$$v_y = \frac{b_1 v_{d,[a_1 b_1 c_1]}}{\sqrt{(a_1^2 + b_1^2 + c_1^2)}} + \frac{b_2 v_{d,[a_2 b_2 c_2]}}{\sqrt{(a_2^2 + b_2^2 + c_2^2)}} + \frac{b_3 v_{d,[a_3 b_3 c_3]}}{\sqrt{(a_3^2 + b_3^2 + c_3^2)}} \quad (3.20)$$

$$v_z = \frac{c_1 v_{d,[a_1 b_1 c_1]}}{\sqrt{(a_1^2 + b_1^2 + c_1^2)}} + \frac{c_2 v_{d,[a_2 b_2 c_2]}}{\sqrt{(a_2^2 + b_2^2 + c_2^2)}} + \frac{c_3 v_{d,[a_3 b_3 c_3]}}{\sqrt{(a_3^2 + b_3^2 + c_3^2)}}$$

As $[a_1,b_1,c_1]$, $[a_2,b_2,c_2]$ and $[a_3,b_3,c_3]$ are mutually perpendicular direction we have,

$$a_1 a_2 + b_1 b_2 + c_1 c_2 = 0$$

$$a_1 a_3 + b_1 b_3 + c_1 c_3 = 0 \quad (3.21)$$

$$a_3 a_2 + b_3 b_2 + c_3 c_2 = 0$$

For N electrons in the simulation the average drift velocity is then calculated as

$$\langle v_x \rangle = \frac{1}{N} \sum_{i=1}^{N} v_{x,i}$$

$$\langle v_y \rangle = \frac{1}{N} \sum_{i=1}^{N} v_{y,i} \quad (3.22)$$

$$\langle v_z \rangle = \frac{1}{N} \sum_{i=1}^{N} v_{z,i}$$

where $v_{x,i}$, $v_{y,i}$ and $v_{z,i}$ are the drift velocities of the i^{th} electron in the x,y and z directions and will depend on the sub-valley the electron is in at the time of the calculation.

Since it is a Monte Carlo simulation, there is always a certain amount of error in the final velocities even when steady state is reached. Therefore simply taking the last value of the steady state velocity is inaccurate. Similar conclusion holds for the average energies as well. Therefore an average is taken in the last ‘t’ seconds of the simulation over all the quantities and it is this average over time ‘t’ that is used to plot the velocity versus electric field plots to extract the mobility or the energy versus electric field plots. The amount of time ‘t’ used to take the average is a user defined value. It is usually one or two picoseconds after steady state is reached.

CHAPTER 4. RESULTS

The generalized Monte Carlo code was used to reproduce the characteristic results of certain materials to test its capability. There are a set of parameters for each material which are fitting parameters used to best fit the simulated data to the experimental data.

4.1. Silicon

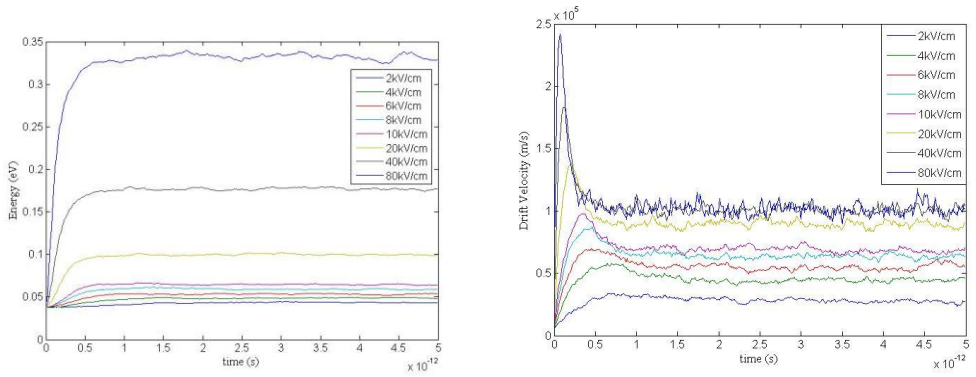

Figure 4.1 Energy of electrons in eV versus time in seconds (left panel) Drift velocity the of electrons in m/s versus time in seconds (right panel)

In figure 4.1 the usual plots of energy versus time and velocity versus time are shown. As can be seen steady state is achieved quite fast at around 2ps. In figure 4.1 the saturation of the velocity with the increase in electric field can be seen with the last two values of electric field plotted.

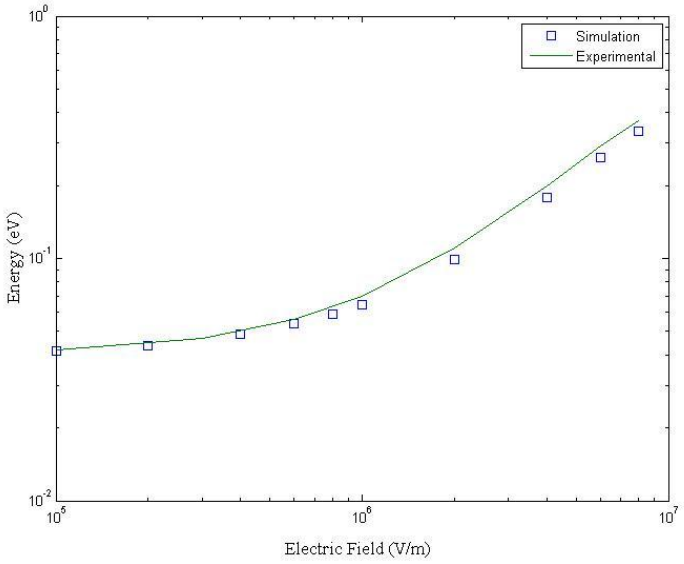

Figure 4.2 Energy of the electrons versus the applied electric field. Experimental data is taken from [29].

In figure 4.2 the velocity for different electric fields is plotted and compared with experimental data. As can be seen there is very good agreement between the experimental values and the values obtained from the simulation.

In figure 4.3 a similar plot is plotted between energy and electric field. In all these plots the electric field is applied in the [111] direction. As can be seen again there is a very good agreement between the experimental values and those obtained from the simulation.

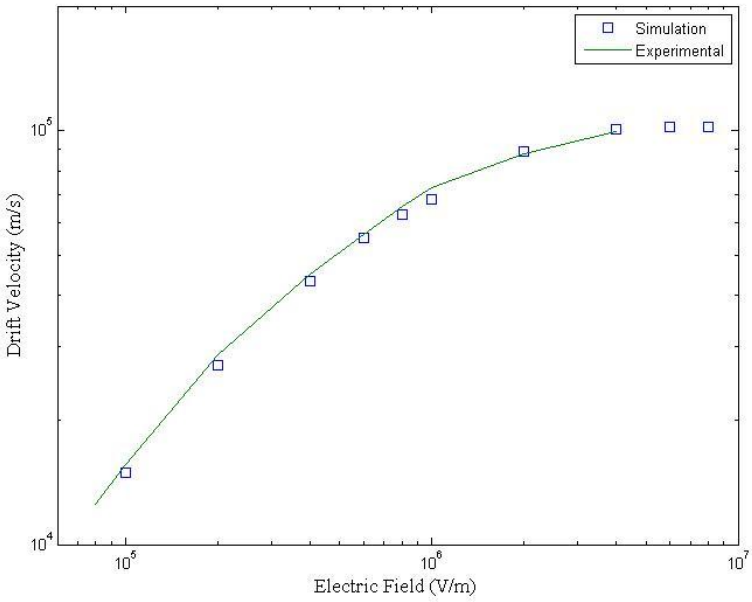

Figure 4.3 Drift velocities of the electrons versus the applied electric field. Experimental data is taken from [29].

4.2. Germanium

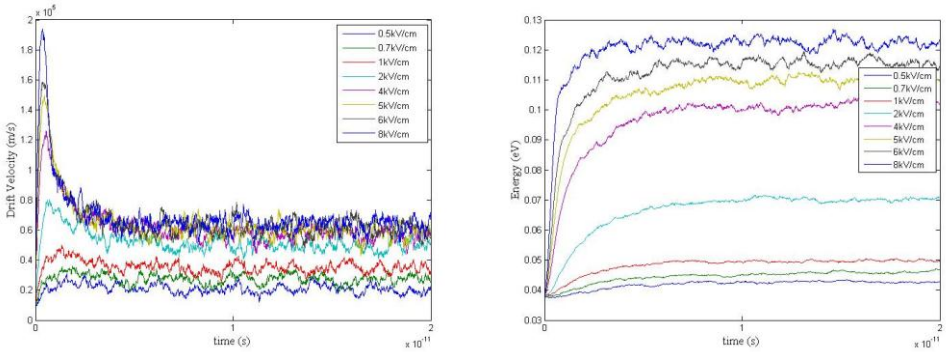

Figure 4.4 Drift velocity versus time for Germanium

The velocity of the electrons and the energy of the electrons are plotted against time in figure 4.4. In germanium the number of valleys chosen is 3, the L valley, Gamma valley and the X valley. Due to this the simulation takes longer to reach steady state as there will be transfer of electrons between the valleys and a transfer of energy between the valleys. This can be seen when these curves are compared with those obtained with silicon which uses just 1 valley (the X valley) in the previous section.

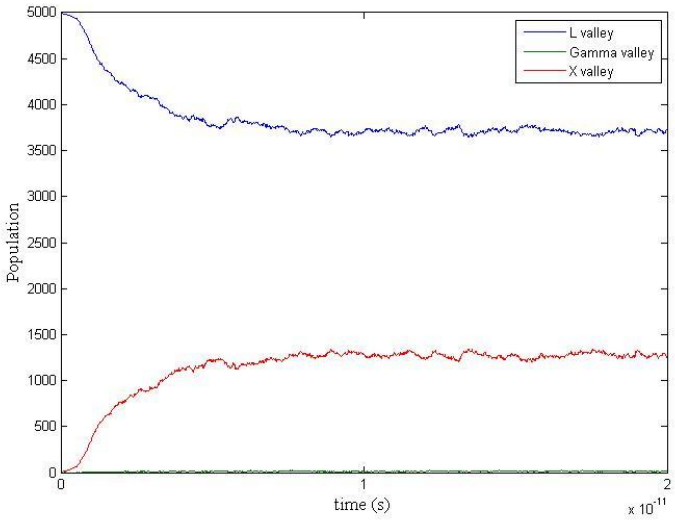

Figure 4.5 Population of Valleys versus time at 6kV/cm in Germanium

In figure 4.5 the number of electrons in each valley is plotted versus time. As can be seen there are almost no electrons in the gamma valley as its effective mass is really small. This causes a low density of states causing a low probability of scattering into that valley.

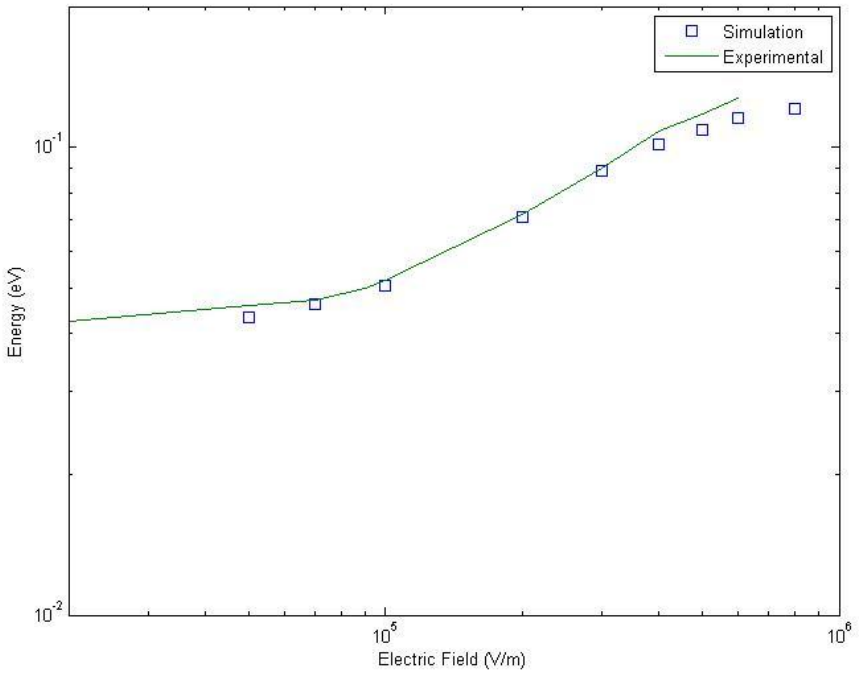

Figure 4.6 Energy versus Applied electric field in Germanium. Experimental data is taken from [30].

In figure 4.6 and figure 4.7 the energy of the electrons and the steady state drift velocity of the electrons are plotted against the applied electric field and compared with experimental values. As can be seen there is a good agreement between the experimental data and the simulated data. It is also possible to obtain even more accurate results by tweaking the fitting parameters further more.

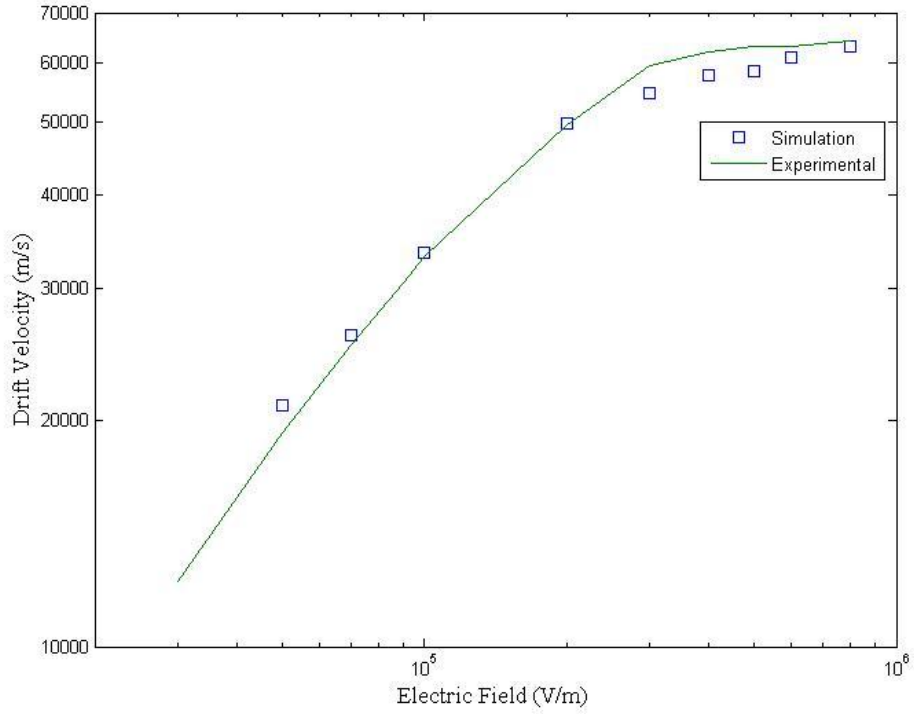

Figure 4.7 Drift velocity versus applied electric field in Germanium. Experimental is data taken from [30].

4.3. Gallium Arsenide

In figure 4.8 the drift velocity and the energy of the electrons are plotted against time. Just as is the case in germanium, in gallium arsenide there are 3 valleys. Therefore the simulation takes a longer time to reach steady state as can be seen in these two figures. In figure 4.9 and figure 4.10 the energy of the electrons and the steady state drift velocity of the electrons are plotted against the applied electric field and compared with experimental values. In figure 4.11 the fraction of electrons in the L valley is plotted against the applied electric field.

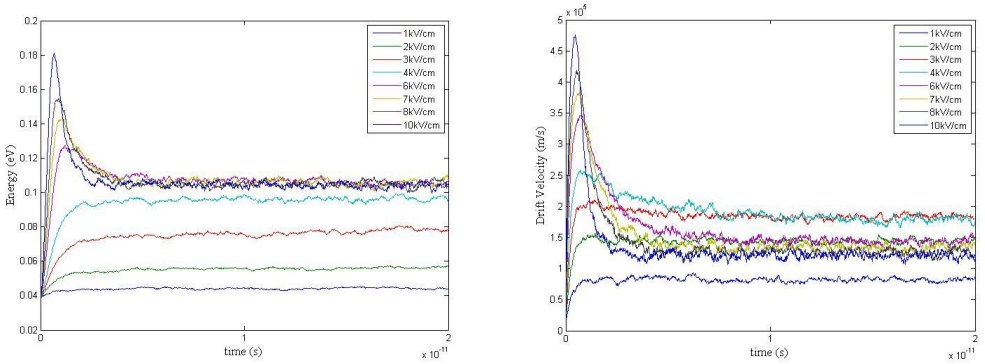

Figure 4.8 Energy versus time in Gallium Arsenide

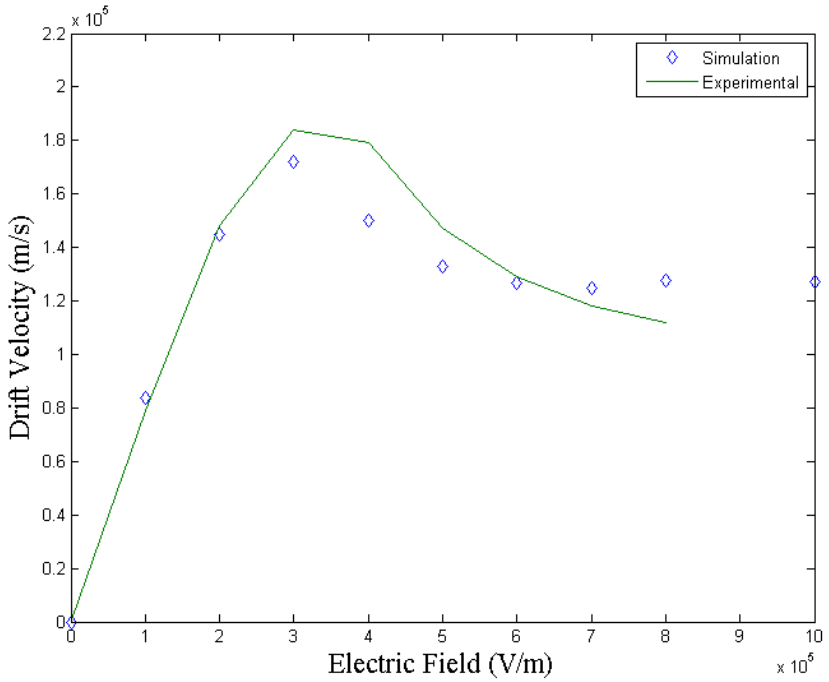

Figure 4.9 Drift velocity of electrons versus applied electric field. Experimental data is taken from [31].

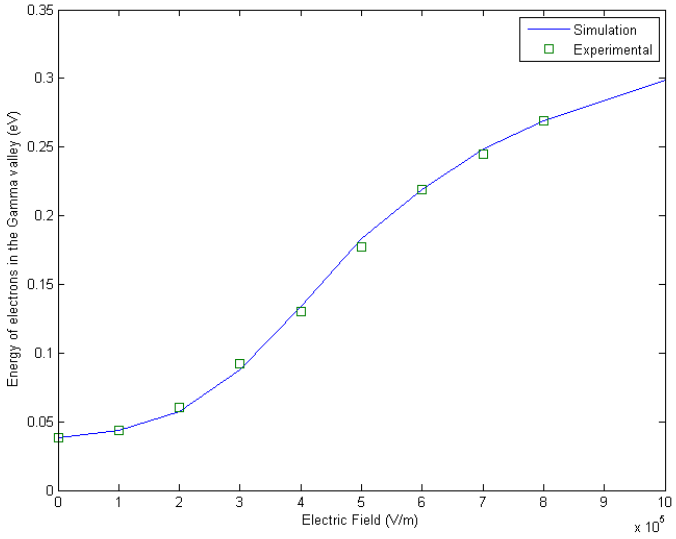

Figure 4.10 Energy of electrons in the gamma valley versus applied electric field. Experimental data is taken from [32].

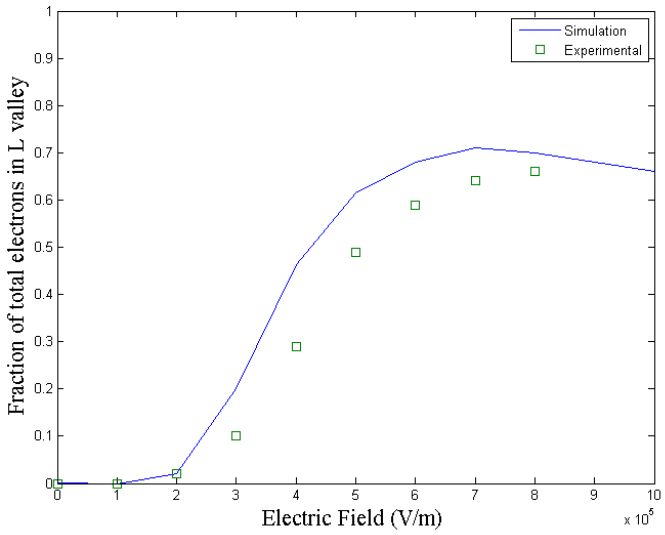

Figure 4.11 Fraction of electrons in the L valley versus applied electric field. Experimental data is taken from [32].

CHAPTER 5. THE RAPPTURE INTERFACE

5.1. Introduction

Rappture is a toolkit supporting rapid application infrastructure, making it quick and easy to develop powerful scientific applications. The Rappture toolkit provides the basic infrastructure for a large class of scientific applications, letting scientists focus on their core algorithm when developing new simulators [33]. The tools on www.nanoHUB.org were created using Rappture as the user interface making the code easily useable and accessible to most people. The same was done for the generalized bulk Monte Carlo tool.

5.2. Input Parameter Structure

The material can have up to 4 different valleys with each having up to 12 different sub-valleys (equivalent valleys). The Rappture interface is designed to facilitate the process of entering such a large number of inputs. Some parameters are not required for certain materials while others are. The tool also has the option of pre-loading a material's input parameters so that the user can run the simulation of a known material and examine the output. As can be seen in Figure (5.1), the user can choose the material from the drop down menu and the values will automatically load themselves. Additional materials can be easily added to the tool after the fitting parameters have been carefully selected to match experimental data.

Figure 5.1 Material Parameters

The tool guides the user across the various parameters required before starting the actual simulation. Any electric field direction can be chosen. The other parameters that can be chosen are also listed. One can also speed up the simulation by reducing the maximum energy of the scattering table if a low field simulation is running, or by reducing the number of electrons simulated. As can be seen in Figure (5.2) there is also the option to choose multiple electric fields

each with its own simulation time to output velocity versus field/ energy versus field/ population versus field curves. The tool uses the previous electric field's simulation final carrier distribution as the starting distribution of the new electric field simulation. This means that the new simulation need not be run for a long time as it will reach steady state faster. This speeds up the total time of the simulation which is critical in Monte Carlo simulations.

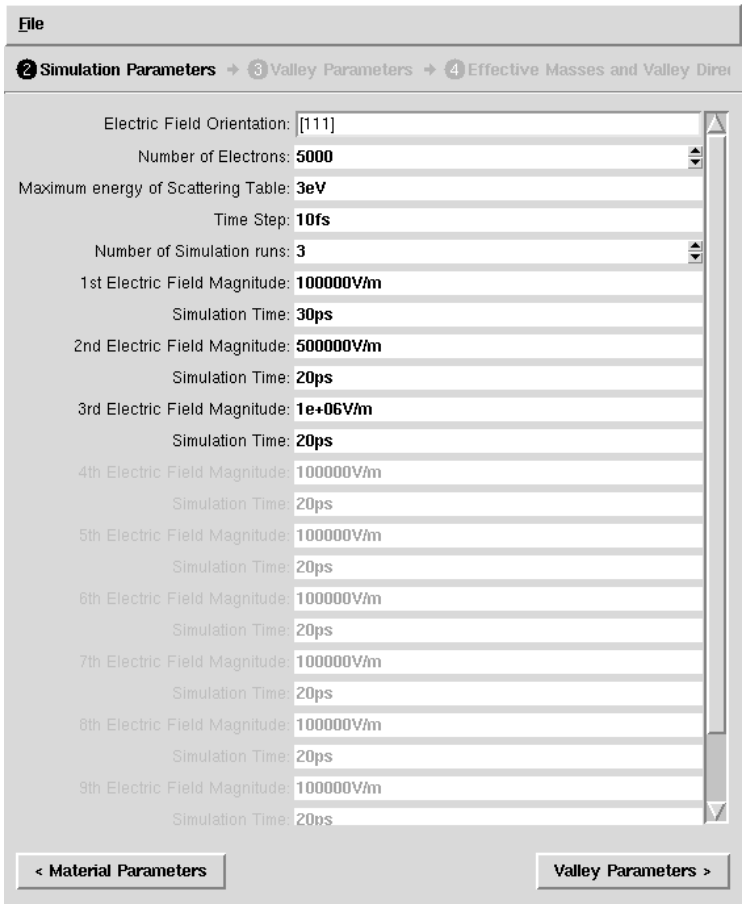

Figure 5.2 Simulation Parameters

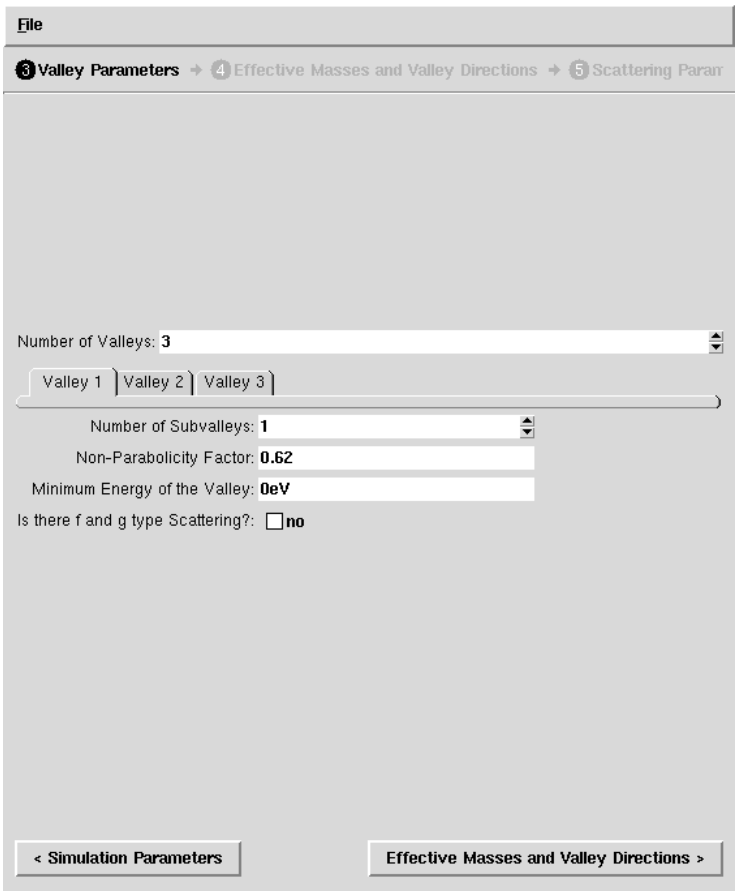

Figure 5.3 Valley Parameters

The valley parameters tab is shown in figure 5.3. The Valley Parameters tab allows the user to choose the number of valleys and the properties of those valleys. The number of valley tabs shown depends on the number of valleys chosen so as to not clutter the page with too much unnecessary information. The same is done with the number of sub-valley tabs below. There is also the option to choose whether the valley has f and g type scattering as in Silicon or not as in

GaAs. The lowest valley is given a minimum energy and the electrons are initially all placed in the lowest energy valley.

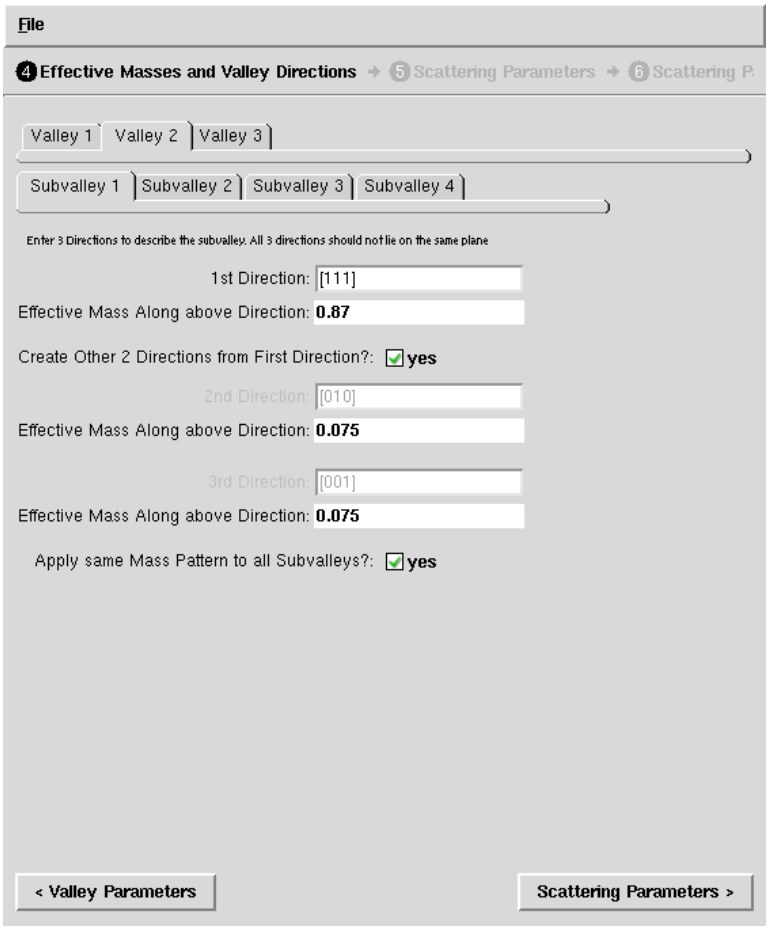

Figure 5.4 Effective masses and Valley directions

To further simplify the input process there are options to let the simulator calculate the transverse directions of the sub-valley so that users are not trying to calculate 3 mutually perpendicular directions. This is shown in figure 5.4. There

is also an option to apply the same mass pattern of the 1st sub-valley to the other sub-valleys if they are all equivalent. Once these options are ticked the information boxes not required are automatically shaded out so as to not confuse the user. So only the parameters required are left open. The above snapshot shows the L valley description of GaAs.

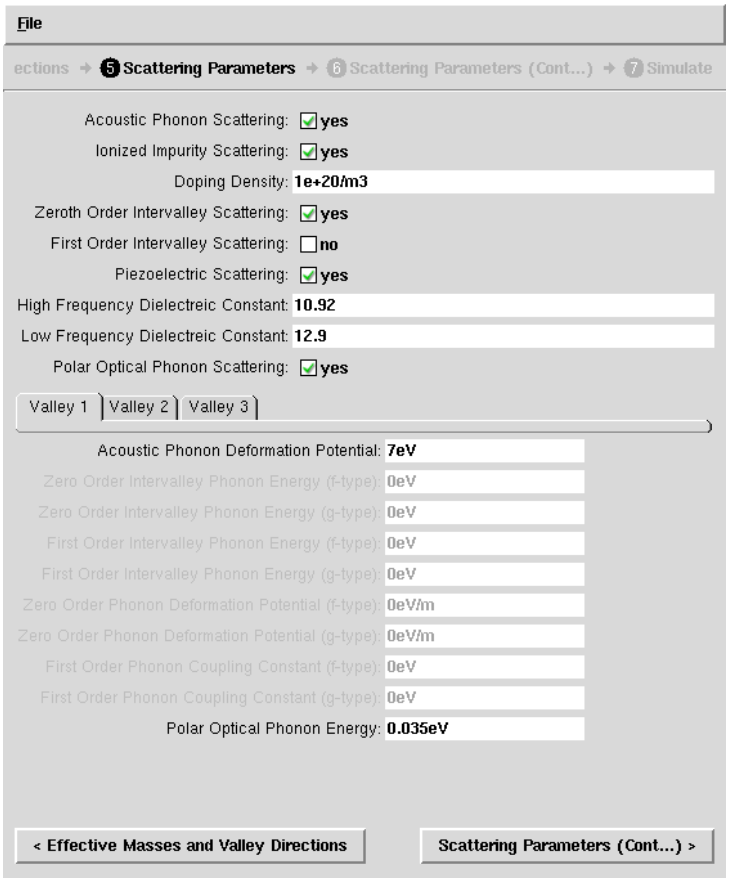

Figure 5.5 Scattering parameters

In this tab (shown in figure 5.5) the user can choose the scattering types, and the relevant parameters required are automatically shown. As in the previous tab the f and g type scattering was not included in Valley 1, all the boxes requiring that information in this valley is shaded out. In this way the user does not get overwhelmed by unnecessary information.

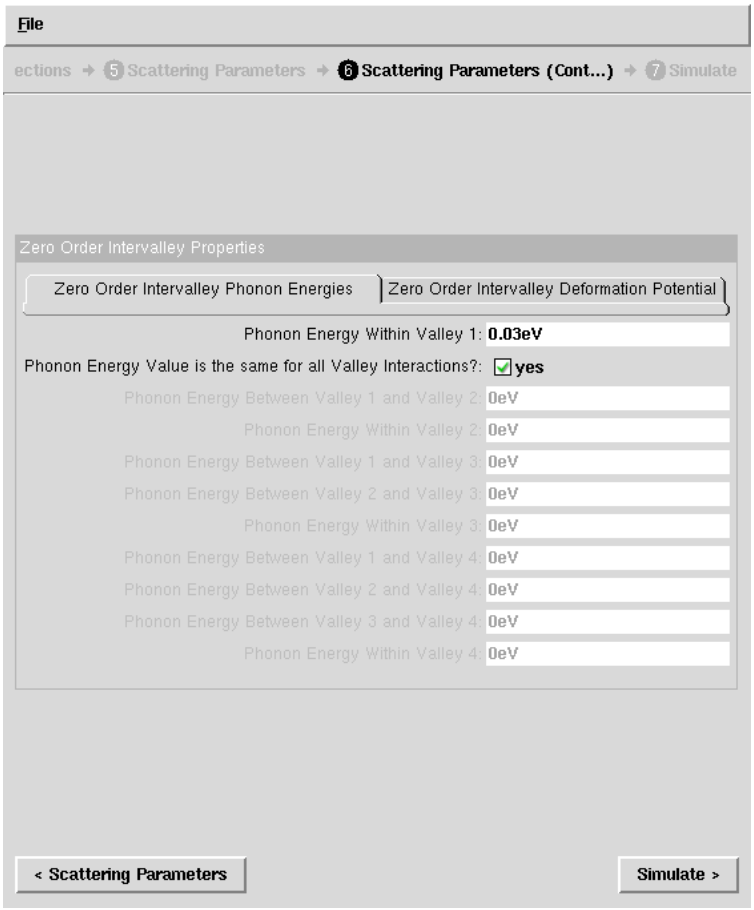

Figure 5.6 Intervalley phonon parameters

Shown in figure 5.6 is the case where only Zero-Order Intervalley Scattering was included and only the information that is required is shown. There is also an

option to allow all valley transitions to have the same phonon energy/deformation potential if needed. There are further adjustments made to the input deck e.g. if f and g type scattering were included in valley 1 there is no need to specify a phonon energy (the independent f and g type phonon energies would have been asked in the previous tab) within the valley , so that option would have been shaded out and so on.

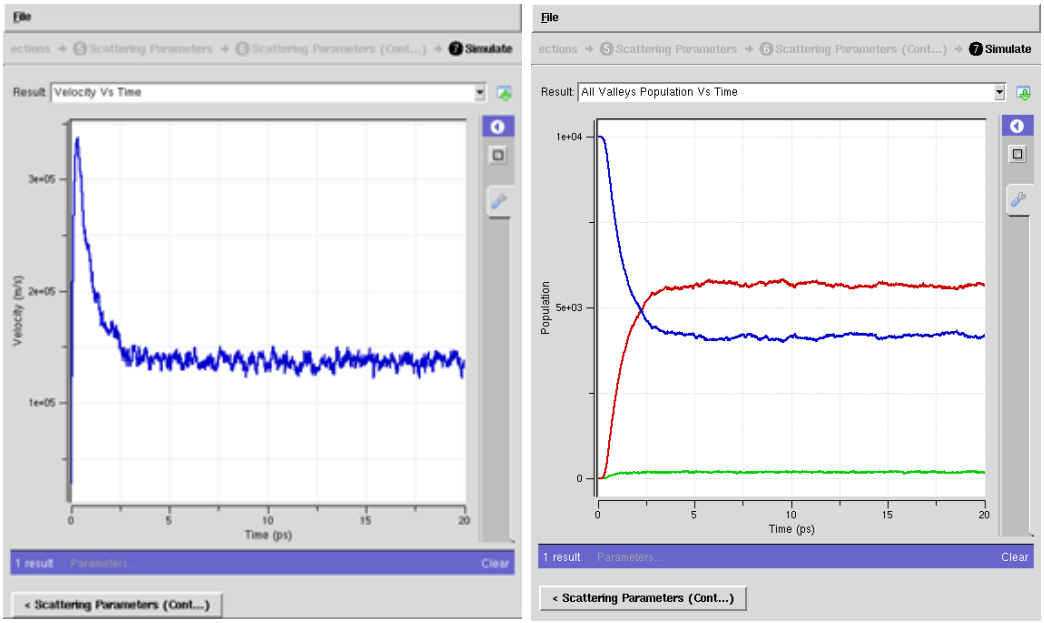

Figure 5.7 Single simulation output of the tool

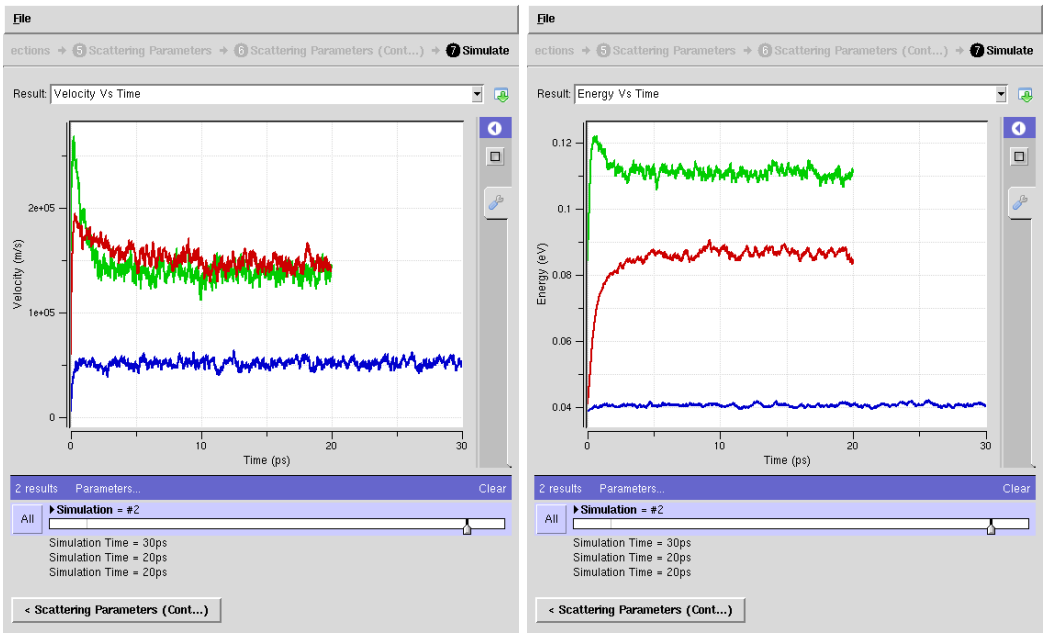

Figure 5.8 Multiple simulation outputs from the tool

Figures 5.7 and 5.8 show the option to run multiple electric fields and observe the output of each electric field to see whether steady state has been achieved. They show the ease in which the user can see whether steady state has been reached or not. The error can also be judged from the outputs which would indicate that the number of electrons used in the simulation may be lacking.

CHAPTER 6. CONCLUSIONS AND FUTURE WORK

This thesis is mainly directed towards creating a research tool and an educational tool. The tool gives the user the option and freedom to vary parameters within limits determined by experimental values of the measured coupling constants and effective masses. Also as this tool will be deployed on www.nanoHUB.org the reach of this tool will be extensive.

The tool uses a non-parabolic band approximation and incorporates most types of scattering rates. As of now it has deformation potential scattering (acoustic and optical), polar optical phonon scattering, piezoelectric scattering and ionized impurity scattering. Using non-parabolic bands makes the simulation as accurate as possible without considering a full band relation. Since it uses an analytical relation between energy and momentum of the electron the simulation time is low, making it more user friendly as an online tool.

The user interface created using the rapture libraries and an xml file can be easily modified to add changes to the tool. This makes updating the tool, which will undoubtedly be needed later, an easy task. Adding new materials to the tool with pre-defined values is also a simple task. The xml file is automatically created and saved every time the user runs the tool meaning that one just has to save the file which has the correct parameters as a new material. This file can then be loaded any time from the drop down menu to simulate that material.

There are some improvements that can be added to this tool. As was mentioned earlier the tool can be easily updated with regard to adding new materials or changing the input interface. There is also a plan to add the scattering rates plots to the output so that the user can see which scattering types dominate and which do not. A possible but not necessary extension of the tool is incorporating a full band simulation instead of the non-parabolic band approximation that was used here. The two have advantages and disadvantages. The non-parabolic band model is definitely not accurate for very high applied fields. But the full band calculation, being an equilibrium calculation is also inaccurate in representing conduction bands, in particular those that lie high in energy. This limitation of the full band models is not always clearly stated in the literature and amongst the scientific community. Modeling of holes with a full-band calculation is a must as holes are accurately represented with a full band structure. Thus adding hole transport with a full-band model is a possible extension of the tool.

REFERENCES

[1] Braun, Ernest; Stuart MacDonald (1982). "*Revolution in Miniature: The history and impact of semiconductor electronics, 2nd Ed*." UK Cambridge Univ. Press 11-12.

[2] Schockley, W. 1951, Bell Syst. Tech. J. 30, 990.

[3] C. Jacoboni and L. Reggiani "*The Monte Carlo method for the solution of charge transport in semiconductors with applications to covalent materials*" 646-703.

[4] Keyes, Robert W. (September 2006). "*The Impact of Moore's Law*". *Solid State Circuits Newsletter*. Retrieved 28 November 2008.

[5] Davydov, B., 1936, *Phys. Z.* Sowjetunion 9, 443.

[6] Davydov, B., 1937, *Phys. Z.* Sowjetunion 12, 269..

[7] Landau, L., and A. Kompanejez, 1934, *Phys. Z.* Sowjetunion 6, 163.

[8] Gunn, J. B., 1963, *Solid State Commun*. 1, 88.

[9] Kurosawa, T., 1966, in *Proceedings of the International Conference on the Physics of Semiconductors*, Kyoto, *J. Phys*. Soc. Jpn. Suppl. 21, 424.

[10] Budd H., 1966, in *Proceedings of the International Conference on the Physics of Semiconductors*, Kyoto, *J. Phys*. Soc. Jpn. Suppl. 21, 420.

[11] Price, P. J., 1968, in *Proceedings of the 9th International Conference on the Physics of Semiconductors*, edited by S. M. Ryvkin, p. 173.

[12] Rees, H. D., 1969, *J. Phys. Chem. Solids* 30, 643.

[13] Fawcett, W., D. A. Boardman, and S. Swain, 1970, *J. Phys. Chem. Solids* 31, 1963.

[14] A.K. Saxena, M. Mudares, *Journal of Applied Physics*, Vol.58 Issue 7.

[15] Buslenko, N. P., D. I. Golenko, Yu. A. Schrieder, I. M. Sobol, and V. G. Sragovich, 1966, "*The Monte Carlo method: The Method of Statistical Trials*", Vol. 87.

[16] Meyer, H. A., 1956, Ed. *Symposium on Monte Carlo methods* (Wiley, NY).

[17] Marchuk, G. I., G. A. Mikhailov, M. A. Nazaraliev, R. A. Darbinjan, B. A. Kargin, and B. S. Elpov, 1980, "*The Monte Carlo Methods in Atmospheric Optics*," Vol. 12 of Springer Series in Optical Sciences (Springer, Berlin).

[18] D. K. Ferry, "*Semiconductors*" (Macmillan, New York, 1991).

[19] K. Tomizawa, "*Numerical Simulation of Submicron Semiconductor Devices*", (Artech House, Boston, 1993).

[20] H. D. Rees, *J. Phys*. C5, 64 (1972).

[21] H. D. Rees, *Solid State Commun*. A26, 416 (1968).

[22] D. Vasileska, S. M. Goodnick, "*Computational Electronics*" , Morgan and Claypool.

[23] "*Semiconductor Transport*", D. Vasileska, http://vasileska.faculty.asu.edu/EEE534.html.

[24] M. Costato, *J. Phys. C: Solid State Phys.* **5** 159 (1972).

[25] J. Bardeen and W. Schockley, *Phys. Rev*. B, 80, 72-80 (1950).

[26] D. K. Ferry, *Phys. Rev. B*, Vol. **14**, 1605 (1976).

[27] C. Trallero Giner and F. Comas, *Phys. Rev. B,* 37, 4583-4588 (1988).

[28] Karl Hess, "*Monte Carlo device simulation: full band and beyond*", Kluwer Academic Publishers.

[29] Jacoboni, C., C. Canali, G. Ottaviani, and A. A. Quaranta, *Solid State Electron.* 20, 2(1977) 77-89.

[30] Jacoboni C., F. Nava, C. Canali and G. Ottaviani, Phys. Rev. B24, 2 (1981) 1014-1026.

[31] Blakemore, J. S., *J. Appl. Phys.* **53**, 10 (1982) R123-R181.

[32] Pozhela, J. and A. Reklaitis, *Solid State Electron.* **23**, 9 (1980) 927-933.

[33] Michael McLennan (2005), "*Add Rappture to Your Software Development*," http://nanohub.org/resources/240.